Limiting etioplast gene-expression induces apical hook twisting during skoto-morphogenesis of Arabidopsis seedlings

Salek Ahmed Sajib, Björn Grübler, Cylia Oukacine, Etienne Delannoy, Florence Courtois, Caroline Mauve, Claire Lurin, Bertrand Gakière, Thomas Pfannschmidt, Livia Merendino

Merendino Livia (Orcid ID: 0000-0003-1593-5442)

Limiting etioplast gene-expression induces apical hook twisting during skoto-morphogenesis of *Arabidopsis* seedlings

Salek Ahmed Sajib[1,2] †, Björn Grübler[3]†, Cylia Oukacine[1,2], Etienne Delannoy[1,2], Florence Courtois[3], Caroline Mauve[1,2], Claire Lurin[1,2], Bertrand Gakière[1,2], Thomas Pfannschmidt[4], Livia Merendino[1,2]

†Salek Ahmed Sajib and Björn Grübler should be considered as joint first author

[1] Université Paris-Saclay, CNRS, INRAE, Université Evry, Institute of Plant Sciences Paris-Saclay (IPS2), 91190 Gif sur Yvette, France.

[2] Université Paris-Cité, CNRS, INRAE, Institute of Plant Sciences Paris-Saclay (IPS2), 91190, Gif sur Yvette, France

[3] Univ. Grenoble Alpes, CNRS, INRAE, CEA, IRIG-LPCV, 38000, Grenoble, France

[4] Institut for Botany, Plant Physiology, Leibniz University Hannover, Herrenhäuser Str. 2, 30419 Hannover, Germany

* These authors contributed equally

To whom correspondence may be addressed:
Livia Merendino, E-mail: livia.merendino@universite-paris-saclay.fr; ORCID: 0000-0003-1593-5442

Running Head

Etioplast dysfunction reprograms morphogenesis

This article has been accepted for publication and undergone full peer review but has not been through the copyediting, typesetting, pagination and proofreading process which may lead to differences between this version and the Version of Record. Please cite this article as doi: 10.1111/tpj.16134

Summary

When covered by a layer of soil, seedling development follows a dark-specific program (skoto-morphogenesis) consisting of small, non-green cotyledons, a long hypocotyl and an apical hook to protect meristematic cells. We recently highlighted the role played by mitochondria in the high energy-consuming reprogramming of *Arabidopsis* skoto-morphogenesis. Here, the role played by plastids, another energy supplying organelle, in skoto-morphogenesis is investigated. This study was conducted in dark conditions to exclude light signals so as to better focus on those produced by plastids. It was found that limitation of plastid gene-expression (PGE) induced an exaggerated apical hook bending. Inhibition of PGE was obtained at the level of transcription and translation using the antibiotics rifampicin and spectinomycin, respectively, as well as plastid RPOTp RNA polymerase mutants. Rifampicin-treated seedlings also showed expression induction of marker nuclear genes for mitochondrial stress, perturbation of the mitochondrial metabolism, increase of ROS levels and an augmented capacity of oxygen consumption by mitochondrial alternative oxidases (AOX). AOX enzymes act to prevent over-reduction of the mitochondrial electron transport chain. Previously, we reported that AOX1A, the main AOX isoform, was a key component in the developmental response to mitochondrial respiration deficiency. In this work, we suggest the involvement of AOX1A in the response to PGE dysfunction and propose the importance of signalling between plastids and mitochondria. Finally, it was found that seedling architecture reprogramming in response to rifampicin was independent of canonical organelle retrograde pathways and the ethylene signaling pathway.

Keywords: skoto-morphogenesis, apical hook bending, plastids, mitochondria, gene-expression, ROS, AOX1A, rifampicin, spectinomycin, *Arabidopsis thaliana*.

Significance statement

In underground germination conditions, seedling development follows a dark-specific program (skoto-morphogenesis) consisting of small and non-green cotyledons, a long hypocotyl and an apical hook to protect meristematic cells. We show that skoto-morphogenesis is reprogrammed when plastid gene expression is perturbed leading to an exaggeration of apical hook bending. We propose the involvement of the cooperation between plastids and mitochondria, the energy-supplying organelles of the cell.

Introduction

Plastids are cell organelles in plants that according to the tissue, display large morphological and functional variations (Liebers *et al.*, 2017). Most of these plastid types can interconvert upon environmental- and/or development-induced changes in plant tissues. For example, in the presence of light, undifferentiated (proplastids) or dark-differentiated (etioplasts) plastids become chloroplasts that are characterized by a complex internal structure of membranes, the thylakoids that house chlorophyll-containing proteins and photosynthetic complexes. The photosynthetic process produces ATP, reducing power and sugars/carbon-skeletons that are supplied to the cell. Etioplasts contain prolamellar bodies and complexes containing protochlorophyllide (Pchlide), NADPH and light-dependent NADPH:Pchlide oxidoreductase. In general, the morphological and functional conversions among plastid types are only possible by changes in plastid proteome composition. The plastid proteome is encoded by both plastid and nuclear genomes. This is due to the fact that during their evolution from symbiotic photosynthetic bacteria to cellular organelles, plastids lost most of the original genetic information that was transferred to the nuclear genome. Through a pathway that is referred to as anterograde, the nucleus codes for plastid proteins and controls plastid physiology. However, plastids contain their own genome and because of their prokaryotic origin, the machinery dedicated to the expression of the plastid genome shares many similarities with the bacterial counterpart and so it is sensitive to antibiotics. In *Arabidopsis thaliana* plants, the plastid genome is transcribed by two different types of RNA polymerases, PEP (Plastid-Encoded RNA Polymerase) and NEP (Nucleus-Encoded RNA Polymerase) in combination with different types of factors (Pfannschmidt *et al.*, 2015). PEP is of the eubacterial-type and it can be blocked by antibiotics such as rifampicin. PEP being the only eubacterial RNA polymerase in the cell, this antibiotic is a highly specific inhibitor of PEP-dependent plastidial transcription. PEP transcriptional activity and specificity are regulated by six nucleus-encoded sigma factors and require the presence of nucleus-encoded PEP Associated Proteins (PAPs). In addition, two NEP RNA polymerases, RPOTmp and RPOTp, participate to plastid genome transcription. RPOTp is exclusively localized in plastids whereas RPOTmp is targeted to both plastids and mitochondria. These phage-type enzymes are insensitive to antibiotics. For the plastid translational machinery, the majority of the components are plastid-encoded and eubacterial-like (70S type-ribosomes) but plastid-specific nucleus-encoded factors are also involved (Marín-Navarro *et al.*, 2007). Plastid translational processes can be blocked by several

antibiotics, such as spectinomycin and lincomycin, that specifically affect the 30S and 50S subunits of plastid ribosomes, respectively (Ellis *et al.*, 1970).

Mitochondria are the site of cellular respiration. Like plastids, they are also semi-autonomous organelles of prokaryotic origin, containing their own genome but depending on the nucleus for the expression of their proteins. Concerning the mitochondrial gene-expression machinery, two NEP RNA polymerases are responsible for transcription of the mitochondrial genome; RPOTm, which is exclusively found in mitochondria, and RPOTmp which is also targeted to plastids. They are phage type enzymes, like RPOTp, and therefore insensitive to antibiotic treatments. On the other hand, mitochondrial ribosomes are of the prokaryotic type.

If the nucleus controls the physiology of both plastids and mitochondria by encoding organelle proteins through anterograde signaling pathways, organelles inform the nucleus about their own state through retrograde signalling pathways. Retrograde signals can be classified as either biogenic or operational (Hernández-Verdeja and Strand, 2018; Wang *et al.*, 2018) according to whether they are generated during organelle biogenesis or from mature organelles, respectively, in response to developmental signals and/or environmental cues. Biogenic signals can be triggered by organelle gene expression. A major effect of plastid retrograde signals is to reduce the expression of PHotosynthesis-Associated Nuclear Genes, PHANGs, including *LHCB1.3* and *RBCS*, whenever chloroplast activity is impaired (Wu and Bock, n.d.). On the other hand, mitochondrial retrograde signals induce the expression of Mitochondrial Dysfunction Stimulon (MDS) genes, including *AOX1A, AT12CYS, NDB4* and *UPOX,* when mitochondria become dysfunctional (Wang *et al.*, 2020). Key signalling factors responsible for organelle communication with the nucleus belong to the Genome UNcoupled (GUN) class for plastids and to WRKY and NAC families for mitochondria. To date, six GUN factors have been characterized (Susek et al., 1993; Woodson et al., 2011). Among them, only in the case of GUN1, the retrograde signal has been shown to be mediated by plastid gene expression (PGE), whereas GUN2-6 are all connected to the tetrapyrrole biosynthesis pathway. Concerning the mitochondrial retrograde pathways, ANAC017 has been shown to control the transcription of a large set of nuclear MDS genes in response to mitochondrial stress and is therefore considered as a master regulator of this specific signaling pathway (Ng *et al.*, 2013; Van Aken, Ford, *et al.*, 2016). However, it is worth mentioning that a wide range of stresses like UV, salt, heat, can induce these genes *via* other transcriptional networks that do not involve ANAC017/ *mitochondrial* retrograde response (*MRR*) pathways (Ng *et al.*, 2014).

During the last decades, many studies have been performed to investigate cross-talk pathways between the nucleus and bioenergetic organelles in light-grown plants. However, in

light conditions it is very difficult to separate the effect of plastid signals from the influence of the light as both target the same genes and act on the same promoter sequences. Only limited studies have been performed with dark-grown seedlings but this would allow a better focus on organelle retrograde pathway by excluding "contaminating" light signals.

When seeds are covered by soil, seedlings develop in the dark and they follow a specific developmental program called skoto-morphogenesis (Mazzella *et al.*, 2014; Gommers and Monte, 2018); exhibiting small, non-green cotyledons, a long hypocotyl and an apical hook that protects meristematic cells during soil emergence. At this early stage of development, cell energy demand is high. Recently, the role played by mitochondria during seedling establishment in the dark was investigated using the *rpoTmp* mutant affected in organelle genome transcription together with other independent mutants defective in cytochrome c oxidase (COX)-dependent respiration (Kühn *et al.*, 2009; Tarasenko *et al.*, 2016). This showed that defects in mitochondrial activity led to a drastic re-programming of *Arabidopsis* seedling architecture (Merendino *et al.*, 2020), characterized by an exaggerated hook curvature and a shortening of the hypocotyl. In addition, *rpoTmp* seedlings activated an alternative oxidase (AOX)-dependent respiratory pathway. AOX, an ubiquinol oxidase, has been shown previously to prevent over-reduction of the respiratory electron transport chain and the formation of harmful reactive oxygen species (ROS) (Vanlerberghe, 2013). Genetic impairment of the main AOX isoform (AOX1A) led to perturbations in the redox state of NAD(P)/H pools and ROS contents as well as in the ATP/ADP ratio, thus highlighting the impact of AOX function on cellular energy budget (Vishwakarma *et al.*, 2014; Jayawardhane *et al.*, 2020). Double mutants affected in RPOTmp and AOX1A enzymes showed that reprogramming of skoto-morphogenesis, and in particular the exaggeration of the apical hook, in response to a respiratory stress was dependent on AOX1A (Merendino *et al.*, 2020). This study strongly suggested that AOX1A was a key component in the developmental response to mitochondrial dysfunction and that the ANAC017-dependent mitochondrial retrograde pathway was at least partially required for the reprogramming of skoto-morphogenesis.

Even if the role of plastids on photo-morphogenesis has been clearly demonstrated (Gommers *et al.*, 2020), the impact of plastid function on skoto-morphogenesis has never been investigated. Although non-photosynthetic, etioplasts can still supply energy to the cell through a process called etio-respiration that allows ATP synthesis *via* electron flow from NAD(P)H coming from the oxidative pentose phosphate pathway to oxygen (Kambakam *et al.*, 2016). In addition to energy related processes, etioplasts are also responsible for the biosynthesis of

hormones that control development. Dysfunctional etioplast gene expression is therefore expected to impact seedling development even in the dark.

The main objective of this current work was to study the impact of defects in specific steps of PGE, transcription and translation, on nuclear gene-expression and seedling skoto-morphogenesis and to determine the potential role played by organelle retrograde and ethylene signaling pathways in the developmental response.

Results

Limitation of plastid transcription and translation alters both skoto- and photo-morphogenesis.

To better understand the impact of PGE limitation on dark-grown seedling morphogenesis, PEP-mediated-transcription and translation steps were blocked in plastids by treatment with specific antibiotics, rifampicin and spectinomycin, respectively. A very strong alteration of skoto-morphogenesis, especially at the level of hook bending (increase of the apical hook angle over 180°, identified as a twisting phenotype), was induced by both antibiotics (Fig. 1A). In addition, a similar modification was detected in *rpoTp* seedlings, deficient in the plastid specific and nucleus-encoded RNA polymerase RPOTp (Hricová *et al.*, 2006; Courtois *et al.*, 2007), suggesting that exaggeration of the hook curvature was not due to pleiotropic effects of the drugs but it was a specific developmental response to plastid gene-expression dysfunction. The twisting phenotype was observed when seeds were submitted to rifampicin treatment either at the beginning of the stratification period, or prior to the exposure time to light required to induce germination or at the beginning of the dark growth phase, thus restricting the effect of the plastid blockage to skoto-morphogenesis *in sensu stricto* (Fig. S1). The PGE limitation-induced twisting phenotype was comparable to that brought about by a treatment with ACC, the direct precursor of ethylene (Fig. 1A). Remarkably, impairment of translation by spectinomycin or treatment of seedlings with ACC also strongly reduced the hypocotyl length, conversely to the neutral effect of rifampicin treatment or the lack of RPOTp in the mutant line.

We also tested the effect of PGE limitation on photo-morphogenesis. Being rifampicin light-sensitive, the impact of PGE inhibition was tested in the dark on the development of constitutive photo-morphogenic mutant *cop1-4* seedlings (short hypocotyl, absence of hook, and cotyledon opening even in the dark (Fig. 1B, see *cop1-4*+DMSO, *cop1-4*)). Measurements of cotyledon opening angles indicated that PGE limitation by rifampicin or spectinomycin as well as ACC treatment impaired cotyledon opening thus suppressing the *cop1* mutant seedling phenotype. A similar interference with photo-morphogenesis has been described already for lincomycin- (another antibiotic targeting plastid translation) and ACC-treated light grown seedlings (Martín *et al.*, 2016).

Limitation of plastid transcription impacts on the expression of nuclear genes linked with mitochondrial biology and on mitochondrial metabolism.

To determine the reprogramming extent of gene expression brought about by the RIF-induced limitation of plastid transcription, we performed an Affymetrix microarray analysis to obtain a whole transcriptomic profiling of etiolated WT seedlings grown in the presence of rifampicin *versus* control conditions. 524 genes (465 nuclear and 59 mitochondrial) genes showed a log2-fold change (FC) >0 with a p-value lower than 0.05; 404 nuclear genes showed a log2FC <0 with a p-value lower than 0.05 (Table S1). Functional grouping of the up- and down-deregulated genes according to the GO term revealed a strong link with gene expression processes, in particular in the mitochondrial compartment (translation, RNA metabolism) and with stress/hormone response (Fig. S2A). The ten most up-regulated genes can be clustered in distinct classes: one group containing markers of mitochondrial stress/targets of the mitochondrial retrograde pathway (*AT12CYS-2* and its co-expression partner *NDB4* (Wang *et al.*, 2016), three *DUF295 Organellar B* genes (Lama *et al.*, 2019) and *SPL2* phospatase (Uhrig *et al.*, 2017)) and a gene involved in general mitochondrial functions, *TOM7-2* (coding for a member of the family of TOM7 translocases of the outer mitochondrial membrane); a gene coding for a chloroplast-localized protein with an oxido-reduction function; a group included genes encoding two proline- and glycine-rich proteins, often involved in stress response (Fig. 2A). Among these ten genes, seven encoded mitochondrial-localized proteins and eight were among the ten most up-regulated genes in the mitochondrial respiration mutant *rpoTmp* (Merendino *et al.*, 2020). In addition, mitochondrial genes were globally over-expressed, probably as a compensation effect for a mitochondrial stress (Fig. 2B, p-value=2.2e-16). The gene-expression induction of the organellar RNA polymerase RPOTmp by the RIF treatment (at5g15700; log2FC=0,551; p-value: 0,028253847, Table S1) could in part explain the over-expression of the mitochondrial genome. On the other hand, as expected for a plastid specific inhibitor of transcription, expression of plastid genes was globally down-regulated (p-value=0.000188). The impact of the rifampicin treatment on the global expression of the different cellular genomes is reported in Fig. 2B.

Microarray analysis indicated that the effect of RIF treatment on gene-expression is quite restricted (only 22 genes with log2FC>2 and 14 genes with log2FC<-2, table S1). To verify the quality of microarray, we analyzed the expression of a selection of genes by RT-qPCR and compared the values obtained with the two techniques (Figure 2C and Figure S2B). The largest differences among the values obtained with the RTqPCR and microarrays are found for RPOB (plastidial) and NAD6 (mitochondrial); in both cases the highest values were found with the

RTqPCR analysis (Figure S2B). However, in general, the expression trend for the selected genes was found to be the same, supporting the reliability of the microarray study.

The expression analyses indicated that the levels of transcripts that are generally considered as PEP-dependent as *atpH, atpA* and *rbcL,* and NEP-dependent as *rpoB* were all affected by the rifampicin treatment that is PEP-specific (Table S1, Figure 2C). In addition, some of the plastid tRNAs that are generally agreed as PEP-dependent were over-accumulated upon rifampicin treatment, either because over-expressed by the NEP machinery, as compensatory mechanism, or for increased stability. The classification of PEP and NEP-dependent genes based on studies performed in light-grown plants is likely not valid in our dark conditions. Finally, the levels of both mitochondrial and nuclear transcripts are either increased or unchanged by the rifampicin treatment supporting that this antibiotic limits specifically plastid transcription.

We also tested the specificity of spectinomycin and found that treatment with this antibiotic decreased the levels of the mitochondrial-encoded protein NAD9 to 70% when normalized using the ATPase amounts, while the signals corresponding to the plastid-encoded S7 protein are almost undetectable (Suppl Fig. 3). These data indicate that spectinomycin blocks specifically plastid translation when supplied to dark grown seedlings.

In addition to the induction of nuclear genes related to mitochondrial biology, RIF treatment is also responsible for metabolic perturbation and in particular for upregulation of intermediates of the mitochondrial TCA process. Metabolic profiling by GC-MS revealed 49 significantly affected metabolites in RIF-treated seedling *versus* control (T-test, p-value 0.05), 47 metabolites increased in abundance and two metabolites decreased (Fig. 2D, Suppl Fig. 4A, Table S3). All glycolytic-related carbohydrates (e.g., sucrose, glucose, fructose, rhamnose, xylose, and maltose) as well as TCA cycle intermediates (including citrate, malate, fumarate, and succinate) were significantly more abundant in the PGE-limited seedlings. This could sign a respiratory defect in relation to an over-reduction of the pyridine nucleotide pool. Supporting this, we found an accumulation in lactate that is as well a signature of mitochondrial respiratory deficiency and a shift to fermentation, as already observed in *rpoTmp* and *atphb3* mutants (Van Aken, Ford, *et al.*, 2016). As mitochondrial perturbation can lead to less ATP synthesis, especially in non-photosynthetic tissues, altering amino-acids levels, we quantified these nitrogen metabolites using OPA-HPLC. Even though the total amino acid content was unchanged (Suppl Fig. 4B), we observed a strong shift in amino-acid metabolism, with decreased amounts of ASN, LYS, GLN that might be a consequence of lack of energy (ATP)

required for their synthesis. On the other hand, the pyruvate-derived branched chain amino acids ALA, LEU, VAL, SER and TRP were accumulated, likely as a consequence of the accumulation of the glycolytic intermediates and the GLY levels were reduced, likely because of a defect in the mitochondrial process producing GLY from SER. Furthermore, a substantial increase in fatty acids (palmitic acid, stearic acid, and malonic acid) was observed in the RIF-treated seedlings. These data point to mitochondrial perturbation in the PGE-limited seedlings. On the other hand, ASP is mostly synthesized in the plastid to sustain *de novo* synthesis of other amino-acids as HSER, LYS, MET, THR. The decrease of ASP levels in RIF-treated seedlings could also be due to plastid dysfunction, determining a decrease in plastid-specific LYS synthesis and transferring the ASP flux towards synthesis of MET and THR that accumulate. These observations can be taken as a signature of plastid dysfunction. Finally, the accumulation of glucose 6 phosphate (G6P) might be also a signature of plastid-specific pentose phosphate pathway dysfunction.

The organellar retrograde pathways that are dependent on either ANAC017 or GUN1 are not involved in the developmental response to PGE dysfunction.

In order to determine if the ANAC017-dependent mitochondrial retrograde signalling pathway was involved in the observed developmental response to antibiotic-mediated PGE limitation, *anac017* mutant seedlings were dark-grown on rifampicin. RT-qPCR analyses showed that genetic impairment of ANAC017-dependent retrograde signalling pathways did not interfere with the nuclear gene expression response (induction of mitochondrial stress marker genes, Fig. 3A). In addition, *anac017* seedlings still showed the developmental response (twisting phenotype) to rifampicin-induced plastid transcriptional limitation (Fig. 3B). To analyze the involvement of the plastid retrograde signalling pathway, *gun1* seedlings were dark-grown on rifampicin and seedling morphogenesis was analyzed (Fig. 3C). Like *anac017* plants, *gun1* seedlings responded at the developmental level (hook twisting) to the rifampicin treatment. We then determined the impact of the rifampicin treatment on the expression of the Photosynthetic Associated Nuclear Genes (PhANGs) that are responsive to the plastid retrograde signaling pathway in light-grown plants. To achieve this, we used the transcriptomic profiling data of etiolated WT seedlings grown in the presence/absence of rifampicin and found that none of the selected genes was differentially expressed in a statistically significant manner (Supp Fig. 5A, BH adj P-value > 0.05).

The EIN2-dependent ethylene signalling pathway is not involved in the developmental response to PGE dysfunction.

The twisting phenotype of seedlings induced by treatment with rifampicin or ACC was comparable, suggesting an eventual role of the ethylene-dependent signaling pathway in the response to the PGE limitation. To test this hypothesis, we observed the skoto-morphogenic profile of ethylene-insensitive mutant *ein2-1* seedlings in the presence of rifampicin. It was found that they still exhibited a twisting phenotype when dark-grown on rifampicin containing medium, whereas the exaggeration of hook bending was no longer detected in the presence of ACC (Fig. 3D). In addition, using the transcriptomic data, none of the selected genes involved in ethylene biosynthesis and signaling were induced in a statistically significant manner (Fig. S5B, BH adj p-value> 0.05) except for ACS4 that showed a log2FC of 2 and the BH adj p-value inferior to 0.05. However, no differences were found in ethylene emission levels when rifampicin-treated seedlings were compared to mock (DMSO) seedlings (Suppl Fig. 5C). In conclusion, such results exclude the involvement of the ANAC017, GUN1 and EIN2-dependent pathways in the observed developmental response to PGE dysfunction.

Genetic disruption of AOX1A impairs the developmental response to PGE limitation.

AOX1A has been shown to play a role in skoto-morphogenesis reprogramming in response to mitochondrial respiration deficiency (Merendino *et al.*, 2020). Here we observed that limitation of PGE by rifampicin induced an increase of AOX gene expression not only at the transcript level (Fig. 3A) but also especially at the protein level (Fig. 4A). High levels of AOX proteins also corresponded to an increase in the AOX capacity (KCN-insensitive respiration, Fig. 4B) but not to the total respiratory O_2 consumption rate in rifampicin-treated seedlings (Suppl Fig. 6). In order to investigate if AOX played a role in the developmental response to PGE limitation, two independent allelic mutants in the *AOX1A* gene, coding for the major AOX isoform in dark-grown seedlings (Merendino *et al.*, 2020), *aox1a-1* and *aox1a-2*, were treated with rifampicin. 40-50% of the mutant seedling population was characterized by the absence of twisted hooks and presented either hook or "comma" phenotype (Fig 4C and Suppl Fig. 7A). The "comma" phenotype is arbitrary defined by the absence of sharp hook bending. Importantly, a much higher percentage of seedlings with hook and comma phenotypes, 70%, was detected when the rifampicin concentration was increased to the double, RIF 400µg/ml. When RIF-treated *aox1a* seedlings presenting twisted, hook or comma phenotypes were exposed to light, they greened (Suppl Fig. 7B), indicating that any of those phenotypes was due to developmental arrest.

Finally, we performed NBT staining to detect the accumulation of ROS and found that the RIF-induced superoxide levels were highly increased by genetic abolishment of AOX1A (Fig. 4D). These data highlight a functional link between PGE limitation, the presence of AOX1A, ROS accumulation and the twisting response.

Discussion

Here it is shown that the early developmental program of dark-grown *Arabidopsis* seedlings is altered when PGE is limited in the presence of either rifampicin or spectinomycin (Figure 1A). Rifampicin is highly specific to the plastid transcription machinery since it targets PEP, the only prokaryotic RNA polymerase in a plant cell (Pfannschmidt and Link, 1994). Microarray and RT-qPCR analyses were performed in this work showing the decrease of many plastid transcripts analyzed in rifampicin-treated seedlings (Figs 2B and C, Table S1). We have also observed that the levels of mitochondrial transcripts are increased and of nuclear transcripts unchanged by the rifampicin treatment and we conclude that rifampicin is specific to plastid transcription. Even though the expression trend was generally the same for most of the analyzed genes, some differences were found among the ratio values obtained with the two techniques (Suppl Fig. 2B). The different values can be due to the use of gene specific primers in RTqPCR analysis and random primers in the microarray study. If with random primers it is not possible to distinguish between transcripts that are synthesized from the two strands of the same DNA matrix (sense and anti-sense RNAs corresponding to the same gene), the usage of gene-specific primers in RTqPCR allows to exclusively detect the sense transcript. We reported that the presence of anti-sense RNAs was particularly an issue in plastids (Grübler *et al.*, 2017). Determination of differences in transcript levels between RIF treatment and control conditions could be biased in micro-arrays by the simultaneous detection of sense and anti-sense RNAs of a specific gene that might present a different expression dependence on the PEP polymerase. In addition, in the microarray analysis, there is always a quite high background. This background weakens the ratio values. This could also explain the absence of statistically significantly differentially expressed plastid genes in the microarray compared to the RTqPCR analysis. In addition to the fact that microarray statistical analysis is more stringent caused by the multiple testing adjustment of p values.

Spectinomycin is an antibiotic that targets the plastid ribosomal machinery. Since the mitochondrial ribosomal machinery is also of the prokaryotic type, it might also be inhibited by this drug. However, the levels of the mitochondrial-encoded protein NAD9 were only decreased to 70% by the treatment with spectinomycin (Suppl Fig. 3), while the ones of the plastid-encoded S7 protein are almost undetectable. Our data indicate that spectinomycin blocks specifically plastid translation when supplied to dark grown seedlings. Treatment of seedlings with either of the two antibiotics tested induced the exaggeration of the apical hook angle (Figure 1A). However, shortening of the hypocotyl was observed only in the case of

spectinomycin. Considering that spectinomycin targets translation of all plastid transcripts while rifampicin inhibits transcription of only the PEP polymerase-dependent plastid genes, the degree of impact on skoto-morphogenesis (only hook over-bending or an additional impact on hypocotyl length) might be related to the degree of plastid gene-expression limitation. The conclusion that the twisting phenotype was specifically induced by blockage of PGE was strongly supported by the observation that apical hooks were over-bended in seedlings mutated in the plastid nucleus-encoded RNA polymerase RPOTp (Figure 1A). Also, in *rpoTp* mutant seedlings transcription of only a subset of plastid genes, in this specific case driven by RPOTp-dependent promoters, was inhibited and the impact was detected exclusively at the hook bending level and not at the hypocotyl length.

The remark that the plastid dysfunction-promoted twisting phenotype was comparable to the ACC-induced apical hook over-bending suggested the involvement of ethylene. However, treatment with rifampicin still affected the architecture of ethylene insensitive *ein-2* mutant seedlings, while in this mutant no effect was detected upon ACC treatment (Figure 3D). In addition, no increase in the accumulation of ethylene (Figure S5C) and transcripts of ethylene responsive genes (apart from ACS4, Figure S5B) could be detected in 3-day-old etiolated WT seedlings treated with rifampicin. Finally, the other traits of the ethylene-induced triple response observed in WT seedlings treated with ACC such as hypocotyl thickening and root shortening were not observed in rifampicin-treated seedlings (Figure 1A). All of these data indicate that the ethylene-dependent signaling pathway is not involved in the developmental reprogramming of skoto-morphogenesis observed in response to rifampicin-induced PGE dysfunction in dark-growth conditions.

It was also found that limitation of PGE by rifampicin and spectinomycin treatments impaired cotyledon separation in the constitutive photo-morphogenic mutant *cop1* in dark-growth conditions (Figure 1B). Recently, it has been shown that lincomycin, another antibiotic targeting plastid translation, impaired cotyledon separation during early development of light-grown WT seedlings (Gommers *et al.*, 2020). Taken together, these data highlight the impact of limiting both plastid transcription and translation on seedling development even when considering different light regime growth conditions. w

To better understand the molecular signalling mechanisms underlying the developmental response to PGE limitation in the dark, the transcriptomic profile of rifampicin-treated seedlings was analyzed using microarrays (Table S1): among the UP DEGs with log2FC>0, there is a very high enrichment (26.9 fold, FDR=4.6E-05) of genes involved in mitochondrial gene-

expression regulation, and more in general with gene-expression processes (Suppl Figure 2A, left panel); among the DOWN DEGs with log2FC<0, there is a very high enrichment of genes involved in stress response (water deprivation 6.3 fold enrichment, FDR=6.4 E-16; hypoxia 6 fold enrichment, FDR=1.3E-08; Suppl Figure 2A, right panel). In addition, six of the top ten most up-regulated transcripts were markers for mitochondrial stress (Figure 2A). In particular, *AT12CYS-2* (At5g09570) was found to be induced mostly in mitochondrial stress condition (Wang *et al.*, 2016; Van Aken and Whelan, 2012). RT-qPCR and western analyses showed that the expression of AOX1A, another marker gene for mitochondrial stress, was clearly induced at both the transcript and protein levels (Fig. 3A and 4A). The stimulation of mitochondrial stress markers and mitochondrial-related genes was surprising for an antibiotic treatment targeting PGE and not mitochondrial gene expression (Figs. 2B and E). However, recent reports have indicated that the expression of marker genes for mitochondrial stress such as *AOX1A* was also induced in response to plastidial stress, as in the case of plants that are treated with methyl viologen, a molecule generating ROS in chloroplasts (Van Aken, De Clercq, *et al.*, 2016) and etiolated *immutans* seedlings lacking plastid terminal oxidase PTOX, an enzyme involved in etio-respiration that is responsible for ATP synthesis in dark-grown seedlings (Kambakam *et al.*, 2016). These data suggest the existence of interacting signaling pathways between organelles and the nucleus. However, the rifampicin-driven twisting phenotype was observed even when ANAC017-dependent mitochondrial retrograde pathways were genetically impaired (Figure 3B). Furthermore, the induction of mitochondrial stress marker genes *AOX1A*, *At12CYS-2* and *NDB4* by rifampicin treatment was not altered by the absence of ANAC017 (Fig. 3A). One interpretation of the data is that an alternative mitochondrial retrograde pathway, independent of canonical factors, is being used when seedlings are subjected to mitochondrial stress in response to plastid dysfunction in the dark. Alternatively, we cannot exclude that induction of stress marker gene expression and of the developmental response does not go *via* a mitochondrial route.

Metabolomics profiling was performed in rifampicin-treated WT Arabidopsis seedlings to determine which metabolites are associated with the PGE limitation and seedling growth (Fig. 2D and Suppl Fig. 4). GC-MS analysis revealed an increase in a number of TCA and glycolytic intermediates in rifampicin-treated seedlings, supporting the idea that rifampicin treatment impacts on mitochondrial metabolism (Fig. 2D). Previous studies have demonstrated that in mitochondrial mutants free amino acids accumulate due to a lack of cellular energy (Van Aken, Ford, *et al.*, 2016). Here, we observed a strong shift in amino-acids metabolism, probably due to a lack of ATP production not compensated by photosynthesis, impairing LYS, ASN and

strongly GLN synthesis (Suppl Fig. 4A). These data support further that RIF interferes with energy production. However, global amino-acid pool remained unchanged (Suppl Fig. 4B). Among shikimate-derived amino-acids, only the anthranilate-branch of the pathway seems to be upregulated, as shown by an increase of TRP levels, and could impact auxin synthesis involved in apical hook formation. Earlier report stated that in the case of mitochondrial dysfunction mutants (*atphb3, rpoTmp*), several other metabolites such as fatty acids and lactic acid are altered (Van Aken, Ford, *et al.*, 2016). Here, we also noticed the accumulation of various fatty acids in the rifampicin-treated seedlings, such as palmitic acid and stearic acid. Specially, lactic acid seems to accumulate, which agrees to the previous report of slowing of aerobic respiration metabolism and a shift to fermentation, which is a classical sign of limited mitochondrial function. Finally, the decrease in GLY can be interpreted as a defect in the mitochondrial process producing GLY from SER. On the other hand, the decrease of ASP and ASP-derived LYS levels could also be due to plastid dysfunction in RIF-treated seedlings, diverging the ASP flux to the synthesis of MET and THR. Finally, the accumulation of glucose 6 phosphate (G6P) might be also interpreted as a sign of dysfunction in plastid-specific pentose phosphate pathway. However, being the G6P also used for 75 to 80% in glycolysis, it is hard to ascertain this hypothesis.

We have also investigated whether the plastid retrograde pathway was involved in the signalling behind the expression and developmental response to PGE limitation. The rifampicin-induced twisting phenotype was observed even when the GUN1 retrograde pathway was genetically impaired (Fig. 3C). Furthermore, the expression levels of canonical gene targets of the plastid retrograde pathway remained unchanged in WT seedling upon rifampicin treatment (Fig. S5A, BH adj p-value>0.05). Therefore, the limitation of plastid transcription by rifampicin does not induce a plastid GUN1-dependent retrograde response in etiolated seedlings. GUN1 protein was recently detected as active in dark (Hernández-Verdeja *et al.*, 2022), but it was not tested if it is involved in PhANGs regulation in response to etioplast deficiency. In addition, since the expression levels of PhANG genes were low in the dark (Grübler *et al.*, 2017), we cannot exclude that an eventual decrease due to the rifampicin treatment might be difficult to detect.
As already reported in the case of mitochondrial stress, accumulation of AOX protein was also induced, together with a concomitant increase of its capacity (measured as KCN-insensitive respiration) in response to plastid dysfunction (Figures 4A and B). Importantly, genetic abolishment of the major AOX1A isoform in the dark partially impaired the developmental response to PGE limitation as seen by a sub-set of rifampicin 200-treated *aox1a-1* and *aox1a-*

2 seedlings, around 40%, being characterized by the absence of a twisted apical hook and presenting either a normal hook (hook) or a round hook (comma, Fig. 4C and Fig. S7A, top and central panels). When the concentration of the RIF was increased to 400 µg/ml, the percentage of seedlings that were unable to twist was larger, around 70%. Interestingly, a similar comma phenotype was also detected when mutant *aox1a* seedlings were treated with spectinomycin (Fig. S7A, bottom panel) and it was previously observed in *aox1a-1/rpoTmp* double mutant seedlings (Merendino *et al.*, 2020). How AOX1A acts to modify seedling architecture during skoto-morphogenesis is still unclear. AOX is an enzyme involved in the control of 1) ROS and nitric oxide (NO) homeostasis by preventing over-reduction of the mitochondrial electron transport chain (Vanlerberghe, 2013) and 2) the redox state of NAD(P)/H pools and ATP/ADP balance, thus influencing cell energy budget (Vishwakarma *et al.*, 2014)(Jayawardhane *et al.*, 2020). We have performed NBT staining to detect ROS accumulation in etiolated seedlings (Fig. 4D). We found that the RIF treatment leads to high ROS levels, especially when AOX1A was genetically abolished. We propose that the ROS produced because of the plastid/mitochondrial stress together with the ones coming from the seeds might inhibit the twisting response. In addition to the involvement in seedling morphogenesis, AOX1A also participates to breaking seed dormancy through the regulation of ROS levels (Jurdak *et al.*, 2020). These concordant results reveal an unexpected role for AOX1A in early steps of plant development (Bailly and Merendino, 2021). However, we cannot exclude that the alteration of the mitochondrial status is just a side effect of the rifampicin treatment and that there is not a functional link between mitochondrial perturbation, AOX1A-depedent ROS accumulation and developmental response of the seedlings.

In conclusion, limitation of PGE by rifampicin and spectinomycin leads to skoto-morphogenesis reprogramming especially at the apical hook bending (Fig. 5). PGE limitation is somehow perceived by the nucleus activating the expression of nuclear genes that are considered as markers for mitochondrial stress such as *AOX1A*. This leads to increased mitochondrial AOX protein amounts and AOX-dependent respiration capacity. In RIF-treated *aox1a* mutant seedlings, we observed a strong accumulation of ROS and the incapacity of a sub-population of seedlings to respond with the twisting phenotype. These data support the involvement of mitochondrial AOX1A in shaping seedling architecture through ROS regulation in a situation of plastid/mitochondrial dysfunction. Finally, rifampicin treatment was also shown to modify the accumulation of mitochondrial metabolic intermediates. Communication from plastids to the nucleus could occur directly or *via* the mitochondria using signals passing

between the organelles, potentially through physical connections. However, the impact on nuclear expression and the developmental response to PGE limitation are independent of GUN1-dependent plastid and ANAC017-dependent mitochondrial retrograde signalling pathways. Finally, the ethylene signalling pathway was shown not to be involved in the skoto-morphogenic reprogramming of the apical hook upon treatment with plastid specific antibiotics.

Experimental procedures

Plant material

Arabidopsis thaliana wildtype (WT) (ecotype Columbia) and mutant lines (*cop1-4* (Deng and Quail, 1992)*; rpoTp* (SALK_067191(Hricová *et al.*, 2006; Courtois *et al.*, 2007)); *ein2-1 (CS3071*(Guzmán and Ecker, 1990)*); gun1-201* (SAIL_290_D09(Martín *et al.*, 2016)); *anac017 (SALK_022174, rao2-1)*[6,7]; *aox1A-1 (*SALK_084897) and *aox1A-2 (SAIL*_030_D08)(Kühn *et al.*, 2015)) were used in this study. Seeds were surface-sterilized and sown on Murashige and Skoog (MS) agar plates supplemented with 1% sucrose and 0.08% charcoal (as a powder to increase image background of etiolated plants, SIGMA-ALDRICH). For chemical treatments, MS agar plates were supplemented with rifampicin (stock of 150 mg/ml in DMSO; SIGMA-ALDRICH R3501; final solution of 100, 200 and 400 µg/ml, it binds to bacterial-like RNA polymerase); spectinomycin (SIGMA-ALDRICH S4014; final solution of 250 or 500 µg/ml, it binds to the ribosomal 30S subunit); 1-aminocyclopropane-carboxylic acid (ACC, SIGMA-ALDRICH A3903, final solution of 20 µM, it is the direct precursor of ethylene). DMSO-containing MS agar plates were used as a mock-control for the rifampicin treatment.

Seeds were stratified for 3 days (at 4°C in the dark), exposed to light (100 $\mu Em^{-2}s^{-1}$ white light) for 6 h and then grown at 23°C in the dark. Plants were either observed or harvested after 3 days.

In the experiment relative to Fig. S1, seeds were sown on nitrocellulose membrane filters (Whatman 10407970, 0.45 µm) either directly on rifampicin-containing MS agar plates at the beginning of stratification or on MS agar plates and then transferred (on the filter) to rifampicin-containing MS agar plates before or after light exposure.

For microarray, RT-qPCR and western-immuno-blot analyses, etiolated plants were harvested in the dark under a green safe-light, immediately frozen in liquid nitrogen, ground in a mortar and subjected to further techniques as described below.

Measurements of phenotypic parameters

Phenotypic appearance of plantlets was analyzed as previously described(Merendino *et al.*, 2020). Briefly, digital images of individual plants were taken with a dissection microscope (Olympus SZX12) using the ACT-1C for DXM1200C software. The angles formed in the apical hook between the hypocotyl and cotyledons were subsequently determined using the ImageJ program (Fig. 1A, lower panel). Any hook angle larger than 180° was considered as twisted. The measurement of the hook angles in RIF-treated mutant *aox1a* seedlings showing a comma phenotype is technically difficult because of the very short and bent hypocotyl (Figure 4C left panel). It is almost impossible to draw a straight line passing through the hypocotyl. That is the reason why we only presented a qualitative analysis of the comma phenotype (Figure 4C right panel). That was already the case for the comma phenotype in the *rpoTmp/aox1a* double mutant (Merendino *et al.*, 2020).

For *cop1-4* mutant seedlings, to determine the cotyledon separation, the angle was measured between cotyledons (Fig. 1B, lower panel).

Statistical analyses of phenotypic parameter measurements

All experimental dataset were tested for the ANOVA assumption of normality of the residuals by both a Normality plot of the residuals and the Shapiro-Wilk test on the ANOVA residuals. Considering that the Shapiro-Wilk test failed, a Wilcoxon test was performed. Statistical analysis was performed using R 4.1.2(Team, 2017).

In Fig 1A all comparisons were significantly different (ANOVA p-values<2e-16). In Fig 1B, the cop mutant was insensitive to RIF200 (Wicoxon p-value >0.05) but impacted by RIF400 (ANOVA p-value <1.7e-11), SPEC (ANOVA p-value <2e-16) and ACC (Wilcoxon p-value<2e-16). In Fig 3B for *anac017*, the response to RIF is even higher than in WT (2-way ANOVA p-value = 7.34e-5). In Fig 3C the *gun1* mutant was not significantly different from WT in both DMSO and RIF treatments (Wilcoxon p-values >0.05). In Fig 3D for *ein2*, the response to RIF 100 or 200 is even higher than in WT for RIF 100 and RIF 200 (2-way ANOVA

p-value = 0.0003 and 0.006). No response to ACC was observed in *ein2* as opposed to WT (2-way ANOVA p-value =1.29e-11).

Microarray analysis

Total RNA purification and microarray analysis were performed as indicated in (Merendino *et al.*, 2020; Grübler *et al.*, 2017). Total RNA was isolated using RNeasy Plant Mini Kit (Qiagen) with on-column DNase I (Qiagen) treatment. Affymetrix whole transcriptome microarray analysis was performed on three biological replicates by the commercial service Kompetenz-Zentrum für Fluoreszente Bioanalytik (KFB) (Regensburg, Germany). cDNAs were prepared using the Ambion® Whole Transcriptome (WT) Expression Kit and fragmented and labeled using the Affymetrix GeneChip® WT Terminal Labeling Kit. Expression analyses were performed using the "GeneChip® Arabidopsis Gene 1.0 ST Array". Since the "Ambion® WT Expression Kit" uses a mixture of oligo-dT and random hexamer primers for the generation of the first strand cDNA, the resulting hybridization signals reflect the accumulation of both organellar and nuclear transcripts.

Statistical analysis of microarray data

Analysis of microarray data was performed as indicated in (Merendino *et al.*, 2020; Grübler *et al.*, 2017). The cell files containing the scanned chips received from KFB were analyzed with RobiNA (Lohse *et al.*, 2012) with the background correction method RMA (robust multi-array average expression measure) (Irizarry *et al.*, 2003), the statistical analysis was performed with Limma (Smyth, 2005) and p-values were adjusted with "nestedF" multiple testing strategy using method Benjamini-Hochberg(Benjamini and Hochberg, 1995). In the analysis using Excel (MS-Office), data with the description "Multiple Hits" were ignored and only results with one-to-one correspondence to a given gene identity were kept for further analysis (Table S1). Microarray data are available at the Gene Expression Omnibus (GEO) under accession number GEO….In Figure S2A, Gene Ontology enrichment analysis of significantly differentially expressed upregulated and downregulated genes (p-value<0.05) was obtained using the ShinyGO software (v.0.76.3, available online: http://bioinformatics.sdstate.edu/go/). No log2FC threshold was applied in this analysis.

In Fig 2B, after microarray normalization, the distributions of the log2FC of the plastid, mitochondrial and nuclear transcripts measured with the microarray were compared using a one-sided Wilcoxon rank sum test (wilcox.test function in R) to find global variations between

each set of transcripts. As the microarray normalization step is applied globally to all genes and that nuclear transcripts are the vast majority of the genes, if the distribution of the organellar transcripts (either plastid or mitochondrial) differs from the distribution of nuclear transcripts then plastid or mitochondrial transcription can be considered to be mis-regulated. In Fig 2B, the log2 FC of mitochondrial transcripts in seedlings treated with RIF were globally higher than nuclear transcripts (Wilcoxon p-value <2e-16). The log2 FC of plastidial transcripts in seedlings treated with RIF were globally lower than nuclear transcripts (Wilcoxon p-value = 4.351e-06).

RT-qPCR analysis of RNA levels

Ground plant material was resuspended in 3 volumes of solution A (10 mM Tris-HCl pH 8.0; 100 mM NaCl; 1 mM EDTA; 1% SDS) and 2 volumes of phenol/chloroform/isoamyl alcohol (25:24:1; v/v/v). After centrifugation, RNAs in the aqueous phase were again extracted twice with phenol-chloroform and finally once with chloroform. After over-night precipitation in 2 M LiCl at 4°C, RNAs were precipitated in ethanol, washed in ethanol 70% and resuspended in water. 500 ng of DNAse (Max Kit, Qiagen) treated-RNAs were retro-transcribed using random hexo-nucleotides or reverse gene-specific primers and the Super-Script II enzyme (Invitrogen) according to the manufacturer´s protocol. The PCR reaction was performed with a Biorad CFX384TM Real Time System PCR machine and forward and reverse gene-specific primers (0.5 µM, Table S2) using the SYBR® Premix Ex Taq™ (Tli RNaseH Plus) from Takara Bio. Data were analyzed using the CFX Manager Software. The expression levels of the transcripts of interest were normalized to the levels of *PP2A* expression, used as a reference gene. The mean values of biological and/or technical replicates were plotted together with the error bars corresponding to standard errors.

Metabolic analyses

Col-0 Arabidopsis seedlings grown in the presence of 200 µg/ml rifampicin and DMSO control were utilized for metabolic profiling using GC-MS. Ground fresh samples (50 mg FW) were resuspended in 1 mL of frozen (-20°C) water:acetonitrile:isopropanol (2:3:3) containing Ribitol at 4 µg mL^{-1} , shaken at 4°C for 10 minutes , centrifuged and 100µl of the SN were dried for 4 hours at 35°C in a Speed-Vac before storing at -80°C. All GC-MS analysis steps were executed as detailed previously (Fiehn, 2006; Fiehn et al., 2008).

For **GC-MS profiling,** the samples were dried again in a Speed-Vac evaporator for 1.5 hours at 35°C before adding 10 µL of 20 mg mL^{-1} methoxyamine in pyridine to the samples and

incubating for 90 minutes at 30°C with continuous shaking. Then, 90 µL of N-methyl-N-trimethylsilyl-trifluoroacetamide (MSTFA) (Regis Technologies, USA) were added and incubated for 30 minutes at 37°C. Then, 100µl samples were transferred to an Agilent vial for injection after cooling. 1µl of sample was injected in split-less mode on an Agilent 7890B gas chromatograph linked to an Agilent 5977A mass spectrometer after 4 hours derivatization where the column was an Rxi-5SilMS from Restek (30 m with 10 m Integra-Guard column). For saturated chemical quantification, an injection in split mode with a ratio of 1:30 was conducted systematically. The oven temperature ramp was 60°C for 1 minute, followed by 10°C min^{-1} to 325°C for 10 minutes. The constant flow of helium was 1.1 mL min^{-1}. Temperatures were as follows: Injector temperature was 250°C, transfer line temperature was 290°C, source temperature was 230°C, and quadrupole temperature was 150°C. After a 5.90-minute solvent delay, the quadrupole mass spectrometer was turned on and scanned from 50 to 600 m/z. Absolute retention times were locked to the internal standard d27-myristic acid using the RTL system provided in Agilent's Masshunter software. Retention time locking decreases the run-to-run variability of retention time. The samples were randomized. In the center of the queue, a mixture of fatty acid methyl esters (C8, C9, C10, C12, C14, C16, C18, C20, C22, C24, C26, C28, C30) was injected for external RI calibration. AMDIS (http://chemdata.nist.gov/mass-spc/amdis/) was used to analyze raw Agilent data files. For metabolite identifications, the Agilent Fiehn GC/MS Metabolomics RTL Library (version June 2008) was used, which is the most comprehensive library of metabolites, comprising GC/MS spectra and retention times for about 700 common metabolites. Peak areas were obtained in splitless and split 30 modes using the Mashunter Quantitative Analysis (Agilent Technologies, CA, USA). Since automatic peak integration can occasionally produce errors, integration was manually validated for each chemical in all analyses. For comparison, the resulting areas were compiled into a single MS Excel file. Ribitol and Dry Weight were used to normalize peak regions. The contents of metabolites were represented in arbitrary units (semi-quantitative determination). All examinations were carried out independently five times. Normalized data (mean-center) were generated into a clustered metabolomic array (heat map) for metabolomics using MeV 4.1 open-source software (Saeed et al., 2003). Metabolites that differed substantially between the two groups were identified using the Student's T-test and a significance value of $P \leq 0.05$.

For amino acids quantification using **OPA-HPLC profiling,** the 200 µL of each sample was dried again in a Speed-Vac evaporator for 1.5 hours at 35°C followed by addition of 1.3 ml H_2O and filtration to inject into the HPLC. The OPA reagent was made 48 h before first use by

dissolving OPA at 10mg/mL in 200 µL of methanol and adding 1.8 mL of sodium borate 0.5M (pH 9.5) and 40 µL of 2-mercaptoethanol. The reagent was filtered into an autosampler vial and used for up to 3 days. Precolumn derivatization was performed in the injection loop by automated mixing of 10 µL sample and 10 µL OPA reagent, followed by a delay of 2 min prior to injection. The HPLC (Alliance Waters 2695, Waters Corporation, USA) fitted with a fluo detector (Multi λ Fluorescence Detector 2475) was used. Compounds were measured at λ excitation of 340nm and λ emission of 455 nm. The chromatographic separation was performed with Symmetry C18 column (3.5µm, 4.6*150 mm) by gradient elution at 40 °C using buffer A (20% methanol, 80% sodium acetate, 1% tetrahydrofuran, pH 5.9) and buffer B (80% methanol, 20% sodium acetate, pH 5.9). Buffer flow rate was 0.8 mL/min throughout and total run time per injection was 42 min. The chromatography data were analyzed by Empower software. Peak identity was confirmed by co-elution with authentic standards. Concentration was calculated with calibration curve using peak area of compound of interest.

Western blot analysis

Total protein extracts were prepared by re-suspending 100 mg of ground plant material in 100 µl of protein lysis buffer (50 mM Tris pH 8.0; 2% SDS; 10 mM EDTA; protease inhibitors (Roche (04693159001) cOmplete™, Mini, EDTA-free Protease Inhibitor Cocktail)) and incubated at room temperature for 30 min. Extracts were cleared by centrifugation for 30 min at 12000 × g at 4°C and dilutions of the supernatant were used to quantify protein amounts with Bradford reagent (SIGMA-ALDRICH B6916). Samples were then denatured for 5 min at 95 °C in 4X reducing electrophoresis sample buffer (200 mM Tris pH 6.8, 5% mercaptoethanol, 4% SDS, 0.2% Bromo Phenol Blue, 20 % glycerol). Comparable amounts of plant protein extracts (100 µg) were separated by SDS-PAGE (12 % acrylamide), electro-blotted onto a nylon membrane that was milk saturated and immuno-decorated with specific polyclonal rabbit antisera against plant mitochondrial alternative oxidase 1 and 2 (AOX1/2; Agrisera, AS04 054), mitochondrial-encoded NAD9 (Lamattina *et al.*, 1993), plastidial-encoded S7 (Agrisera, AS15 2877) and vacuole V-ATPase (Agrisera, AS07 213). The blots were developed with Clarity Western ECL substrate (Bio-Rad, Hercules, USA). Images of the blots were obtained using a CCD imager (Chemidoc MP, Bio-Rad) and the Image Lab program (Bio-Rad, Hercules, USA).

In planta O_2 consumption measurements

Etiolated plantlets were harvested from Petri dishes and immediately soaked in the dark with 1 mL of oxygenated phosphate buffer (10 mM sodium phosphate buffer pH 7.2; 10 mM KCl; 10 mM glucose) in the measurement cell of a Clark oxygen electrode (Hansatech Instruments). For respiratory electron transfer inhibition experiments, KCN (0.1 M stock, inhibitor of COX-dependent pathway at the level of complex IV) and SHAM (0.1 M stock in DMSO, inhibitor of the AOX-dependent pathway) were added directly into the electrode chamber to a final concentration of 1 mM, once the recorded signal reached a constant value. The capacity (or maximum activity) of the AOX-dependent pathway (corresponding to the SHAM-sensitive/KCN-insensitive pathway) and of the COX-dependent pathway (corresponding to the SHAM-insensitive/KCN-sensitive pathway) was calculated as ratio of O_2 consumption rate upon addition of either KCN or SHAM and total O_2 consumption rate (measured in the absence of inhibitors), respectively. The extra mitochondrial O_2 consumption was evaluated at the end of each measurement after addition of both KCN and SHAM and systematically subtracted from O_2 consumption rates.

NBT staining of ROS

Etiolated seedlings were transferred in 12 well plate, vacuum-infiltrated in the dark with 2.5 ml NBT 6 mM staining solution for 5 minutes and incubated for 4h in dark at room temperature with continuous shaking. Digital images of individual plants were taken with a dissection microscope (Olympus SZX12) using the ACT-1C for DXM1200C software.

Ethylene measurements

For ethylene measurements, etiolated seedlings (fresh weight: 500 mg) were collected and put into 5 ml amber, flat bottom screw neck vials (MACHEREY-NAGEL GmbH & Co. KG, Germany Cat no. 702293), and sealed with an N 9 PP screw cap with a center hole and silicone white/PTFE red septum (MACHEREY-NAGEL GmbH & Co. KG, Germany, Cat no. 702287.1). After 4 h, ethylene accumulation measurements were performed with the ETD-300 ET detector (Sensor Sense B.V., Nijmegen, The Netherlands). The accumulated ethylene was drawn through a valve controller over a period of 7 min and with a constant flow of 3L/h and sent into the laser acoustic spectrometer/detector where ethylene was specifically detected. Levels of ethylene emissions are given in ppbv (parts per billion by volume) as a function of the relative time since the start of the experiment.

Acknowledgements: This work was supported by the LabEx Saclay Plant Sciences-SPS (ANR-10-LABX-0040-SPS) to IPS2; grants from the Deutsche Forschungsgemeinschaft [PF323-5-2] and the DFG research group FOR 804; the Centre National de la Recherche Scientifique [PEPS] to TP; the French Ministry of Education and the Grenoble Alliance for Integrated Structural Cell Biology (LabEx GRAL, ANR-10-LABX-49-01) to LPCV. We thank Michael Hodges and Emmanuelle Issakidis-Bourguet from IPS2 (Orsay, France) for helpful discussions; Géraldine Bonnard (IBMP, Strasburg, France) for sharing NAD9 antisera. We thank Olivier Van Aken (Lund University, Sweden) for sharing *anac017* seeds, Fredy Barneche (IBENS, France) for *gun1-201* and *cop1-4* seeds and Kristina Kühn (Universität Halle, Germany) for *aox1a* seeds. RNA sample processing and Affymetrix microarray hybridization were carried out at the genomics core facility: Center of Excellence for Fluorescent Bioanalytics (KFB, University of Regensburg, Germany). SAS was supported by fellowship from the Ministère de l'Enseignement supérieur, de la Recherche et de l'Innovation (MESRI) of French Government (Doctoral School of Plant Sciences (SEVE), Université Paris-Saclay) for his Ph.D.

Author contribution. LM and TP designed research; SAS, BGr, CO, FC, CM and LM performed experiments, ED performed statistical analyses, CL contributed analytical tools. SAS, BGr, FC, CM, BGa, TP and LM analyzed data, LM wrote the manuscript with the help of all co-authors. All authors read and approved the manuscript.

Competing interests. The authors declare no conflict of interest.

Data Statement. Microarray data are available at the Gene Expression Omnibus (GEO) under accession number GSE223240.

Figure S1: The effect of PGE limitation is restricted to skoto-morphogenesis *in sensu stricto.*
Figure S2: Gene expression analysis by RTqPCR and microarray techniques.
Figure S3: Analysis of plastid specificity for the spectinomycin antibiotic.
Figure S4: Schematic representation of metabolite ratio by GC-MS and amino acid quantification by OPA-HPLC in untreated and RIF-treated WT seedlings.
Figure S5: Relative expression values for A) PhANGs and B) genes involved in ethylene biosynthesis and signalling pathways in rifampicin-treated *versus* untreated etiolated WT seedlings.
Figure S6: Total O_2 consumption rate in etiolated WT plants grown in the presence or absence of rifampicin.
Figure S7: Dissection microscope images of etiolated *aox1a-1* and *aox1a-2* seedlings.

References

Aken, O. Van, Clercq, I. De, Ivanova, A., Law, S.R., Breusegem, F. Van, Millar, A.H. and Whelan, J. (2016) Mitochondrial and Chloroplast Stress Responses Are Modulated in Distinct Touch and Chemical Inhibition Phases. *Plant Physiol.*, **171**, 2150–65. Available at: http://www.plantphysiol.org/lookup/doi/10.1104/pp.16.00273 [Accessed May 23, 2018].

Aken, O. Van, Ford, E., Lister, R., Huang, S. and Millar, A.H. (2016) Retrograde signalling caused by heritable mitochondrial dysfunction is partially mediated by ANAC017 and improves plant performance. *Plant J.*, **88**, 542–558. Available at: http://doi.wiley.com/10.1111/tpj.13276 [Accessed May 23, 2018].

Aken, O. Van and Whelan, J. (2012) Comparison of Transcriptional Changes to Chloroplast and Mitochondrial Perturbations Reveals Common and Specific Responses in Arabidopsis. *Front. Plant Sci.*, **3**, 281. Available at: http://www.ncbi.nlm.nih.gov/pubmed/23269925 [Accessed September 11, 2018].

Bailly, C. and Merendino, L. (2021) Oxidative signalling in seed germination and early seedling growth: An emerging role for ROS trafficking and inter-organelle communication. *Biochem. J.*, **478**, 1977–1984.

Benjamini, Y. and Hochberg, Y. (1995) Controlling the False Discovery Rate: A Practical and Powerful Approach to Multiple Testing. *J. R. Stat. Soc. Ser. B*, **57**, 289–300. Available at: https://www.jstor.org/stable/2346101 [Accessed November 18, 2019].

Courtois, F., Merendino, L., Demarsy, E., Mache, R. and Lerbs-Mache, S. (2007) Phage-type RNA polymerase RPOTmp transcribes the rrn operon from the PC promoter at early developmental stages in Arabidopsis. *Plant Physiol.*, **145**, 712–21. Available at: http://www.plantphysiol.org/cgi/doi/10.1104/pp.107.103846 [Accessed May 22, 2018].

Deng, X.-W. and Quail, P.H. (1992) Genetic and phenotypic characterization of cop1 mutants of Arabidopsis thaliana. *Plant J.*, **2**, 83–95. Available at: http://doi.wiley.com/10.1111/j.1365-313X.1992.00083.x [Accessed July 29, 2019].

Ellis, R.J., Mcdonald, I.R., Parenti, F., Margulies, M.M., Schwartz, J.H., Meyer, R., Eisenstadt, J.M. and Brawerman, G. (1970) *Further Similarities between Chloroplast and Bacterial Ribosomes*,.

Gommers, C.M.M. and Monte, E. (2018) Update on Photomorphogenesis Seedling Establishment: A Dimmer Switch-Regulated Process between Dark and Light Signaling 1[OPEN]. *Plant Physiol.*, **176**, 1061–1074. Available at: www.plantphysiol.org/cgi/doi/10.1104/pp.17.01460.

Gommers, C.M.M., Ruiz-Sola, M.Á., Ayats, A., Pereira, L., Pujol, M. and Monte, E. (2020) GENOMES UNCOUPLED1-independent retrograde signaling targets the ethylene pathway to repress photomorphogenesis. *Plant Physiol.* Available at: https://academic.oup.com/plphys/advance-article/doi/10.1093/plphys/kiaa015/5991408 [Accessed February 8, 2021].

Grübler, B., Merendino, L., Twardziok, S.O., et al. (2017) Light and plastid signals regulate different sets of genes in the albino mutant pap7-1. *Plant Physiol.*, **175**.

Guzmán, P. and Ecker, J.R. (1990) Exploiting the triple response of Arabidopsis to identify

ethylene-related mutants. *Plant Cell*, **2**, 513–23. Available at: http://www.plantcell.org/cgi/doi/10.1105/tpc.2.6.513 [Accessed May 22, 2018].

Hernández-Verdeja, T. and Strand, Å. (2018) Retrograde Signals Navigate the Path to Chloroplast Development. *Plant Physiol.*, **176**, 967–976. Available at: http://www.plantphysiol.org/lookup/doi/10.1104/pp.17.01299 [Accessed February 19, 2019].

Hernández-Verdeja, T., Vuorijoki, L., Jin, X., Vergara, A., Dubreuil, C. and Strand, A. (2022) GENOMES UNCOUPLED1 plays a key role during the de-etiolation process in Arabidopsis. *New Phytol.*, **235**, 188–203. Available at: https://nph.onlinelibrary.wiley.com/doi/10.1111/nph.18115 [Accessed January 13, 2023].

Hricová, A., Quesada, V. and Micol, J.L. (2006) The SCABRA3 nuclear gene encodes the plastid RpoTp RNA polymerase, which is required for chloroplast biogenesis and mesophyll cell proliferation in Arabidopsis. *Plant Physiol.*, **141**, 942–956. Available at: www.plantphysiol.org/cgi/doi/10.1104/pp.106.080069.942 [Accessed September 30, 2020].

Irizarry, R.A., Hobbs, B., Collin, F., Beazer-Barclay, Y.D., Antonellis, K.J., Scherf, U. and Speed, T.P. (2003) Exploration, normalization, and summaries of high density oligonucleotide array probe level data. *Biostatistics*, **4**, 249–264. Available at: http://www.ncbi.nlm.nih.gov/pubmed/12925520 [Accessed November 18, 2019].

Jayawardhane, J., Cochrane, D.W., Vyas, P., Bykova, N. V., Vanlerberghe, G.C. and Igamberdiev, A.U. (2020) Roles for Plant Mitochondrial Alternative Oxidase Under Normoxia, Hypoxia, and Reoxygenation Conditions. *Front. Plant Sci.*, **11**. Available at: https://pubmed.ncbi.nlm.nih.gov/32499803/ [Accessed February 12, 2021].

Jurdak, R., Launay-Avon, A., Paysant-Le Roux, C. and Bailly, C. (2020) Retrograde signaling from the mitochondria to the nucleus translates the positive effect of ethylene on dormancy breaking of Arabidopsis thaliana seeds . *New Phytol.* Available at: https://pubmed.ncbi.nlm.nih.gov/33020928/ [Accessed November 3, 2020].

Kambakam, S., Bhattacharjee, U., Petrich, J. and Rodermel, S. (2016) PTOX Mediates Novel Pathways of Electron Transport in Etioplasts of Arabidopsis. *Mol. Plant*, **9**, 1240–1259. Available at: http://www.ncbi.nlm.nih.gov/pubmed/27353362 [Accessed May 29, 2019].

Kühn, K., Richter, U., Meyer, E.H., et al. (2009) Phage-type RNA polymerase RPOTmp performs gene-specific transcription in mitochondria of Arabidopsis thaliana. *Plant Cell*, **21**, 2762–79. Available at: http://www.plantcell.org/cgi/doi/10.1105/tpc.109.068536 [Accessed October 8, 2018].

Kühn, K., Yin, G., Duncan, O., et al. (2015) Decreasing Electron Flux through the Cytochrome and/or Alternative Respiratory Pathways Triggers Common and Distinct Cellular Responses Dependent on Growth Conditions. *Plant Physiol.*, **167**, 228–250. Available at: http://www.ncbi.nlm.nih.gov/pubmed/25378695 [Accessed May 23, 2018].

Lama, S., Broda, M., Abbas, Z., Vaneechoutte, D., Belt, K., Säll, T., Vandepoele, K. and Aken, O. Van (2019) Neofunctionalization of Mitochondrial Proteins and Incorporation into Signaling Networks in Plants M. Purugganan, ed. *Mol. Biol. Evol.*, **36**, 974–989. Available at: http://www.ncbi.nlm.nih.gov/pubmed/30938771 [Accessed July 19, 2019].

Lamattina, L., Gonzalez, D., Gualberto, J. and Grienenberger, J.M. (1993) Higher plant mitochondria encode an homologue of the nuclear-encoded 30-kDa subunit of bovine mitochondrial complex I. *Eur. J. Biochem.*, **217**, 831–8. Available at: http://www.ncbi.nlm.nih.gov/pubmed/8223639 [Accessed May 22, 2018].

Liebers, M., Grübler, B., Chevalier, F., Lerbs-Mache, S., Merendino, L., Blanvillain, R. and Pfannschmidt, T. (2017) Regulatory shifts in plastid transcription play a key role in morphological conversions of plastids during plant development. *Front. Plant Sci.*, **8**.

Lohse, M., Bolger, A.M., Nagel, A., Fernie, A.R., Lunn, J.E., Stitt, M. and Usadel, B. (2012) RobiNA: a user-friendly, integrated software solution for RNA-Seq-based transcriptomics. *Nucleic Acids Res.*, **40**, W622-7. Available at: https://academic.oup.com/nar/article-lookup/doi/10.1093/nar/gks540 [Accessed November 18, 2019].

Marín-Navarro, J., Manuell, A.L., Wu, J. and P. Mayfield, S. (2007) Chloroplast translation regulation. *Photosynth. Res.*, **94**, 359–374. Available at: http://www.ncbi.nlm.nih.gov/pubmed/17661159 [Accessed February 19, 2019].

Martín, G., Leivar, P., Ludevid, D., Tepperman, J.M., Quail, P.H. and Monte, E. (2016) Phytochrome and retrograde signalling pathways converge to antagonistically regulate a light-induced transcriptional network. *Nat. Commun.*, **7**, 11431. Available at: http://www.nature.com/articles/ncomms11431 [Accessed February 11, 2019].

Mazzella, M.A., Casal, J.J., Muschietti, J.P. and Fox, A.R. (2014) Hormonal networks involved in apical hook development in darkness and their response to light. *Front. Plant Sci.*, **5**, 52. Available at: http://journal.frontiersin.org/article/10.3389/fpls.2014.00052/abstract [Accessed May 22, 2018].

Merendino, L., Courtois, F., Grüble, B., Bastien, O., Straetmanns, V., Chevalier, F., Lerbs-Mache, S., Lurin, C. and Pfannschmidt, T. (2020) Retrograde signals from mitochondria reprogram skoto-morphogenesis in Arabidopsis thaliana via Alternative Oxidase 1a. *Philos. Trans. R. Soc. B.*

Ng, S., Clercq, I. De, Aken, O. Van, Law, S.R., Ivanova, A., Willems, P., Giraud, E., Breusegem, F. Van and Whelan, J. (2014) Anterograde and Retrograde Regulation of Nuclear Genes Encoding Mitochondrial Proteins during Growth, Development, and Stress. *Mol. Plant*, **7**, 1075–1093. Available at: http://www.ncbi.nlm.nih.gov/pubmed/24711293 [Accessed January 24, 2019].

Ng, S., Ivanova, A., Duncan, O., et al. (2013) A Membrane-Bound NAC Transcription Factor, ANAC017, Mediates Mitochondrial Retrograde Signaling in Arabidopsis. *Plant Cell*, **25**, 3450–3471. Available at: http://www.ncbi.nlm.nih.gov/pubmed/24045017 [Accessed May 23, 2018].

Pfannschmidt, T., Blanvillain, R., Merendino, L., Courtois, F., Chevalier, F., Liebers, M., Grübler, B., Hommel, E. and Lerbs-Mache, S. (2015) Plastid RNA polymerases: Orchestration of enzymes with different evolutionary origins controls chloroplast biogenesis during the plant life cycle. *J. Exp. Bot.*, **66**.

Pfannschmidt, T. and Link, G. (1994) Separation of two classes of plastid DNA-dependent RNA polymerases that are differentially expressed in mustard (Sinapis alba L.)

seedlings. *Plant Mol. Biol.*, **25**, 69–81. Available at: http://www.ncbi.nlm.nih.gov/pubmed/8003698 [Accessed January 24, 2019].

Smyth, G.K. (2005) limma: Linear Models for Microarray Data. In *Bioinformatics and Computational Biology Solutions Using R and Bioconductor*. New York: Springer-Verlag, pp. 397–420. Available at: http://link.springer.com/10.1007/0-387-29362-0_23 [Accessed November 18, 2019].

Tarasenko, V.I., Katyshev, A.I., Yakovleva, T. V, Garnik, E.Y., Chernikova, V. V, Konstantinov, Y.M. and Koulintchenko, M. V (2016) RPOTmp, an Arabidopsis RNA polymerase with dual targeting, plays an important role in mitochondria, but not in chloroplasts. *J. Exp. Bot.*, **67**, 5657–5669. Available at: http://www.ncbi.nlm.nih.gov/pubmed/27591433 [Accessed May 22, 2018].

Team, R. (2017) R: A language and environment for statistical computing. R Foundation for Statistical Computing, Vienna, Austria. 2016. Available at: https://www.r-project.org [Accessed May 23, 2018].

Uhrig, R.G., Labandera, A.-M., Tang, L.-Y., Sieben, N.A., Goudreault, M., Yeung, E., Gingras, A.-C., Samuel, M.A. and Moorhead, G.B.G. (2017) Activation of Mitochondrial Protein Phosphatase SLP2 by MIA40 Regulates Seed Germination. *Plant Physiol.*, **173**, 956–969. Available at: http://www.plantphysiol.org/lookup/doi/10.1104/pp.16.01641 [Accessed November 13, 2019].

Vanlerberghe, G. (2013) Alternative Oxidase: A Mitochondrial Respiratory Pathway to Maintain Metabolic and Signaling Homeostasis during Abiotic and Biotic Stress in Plants. *Int. J. Mol. Sci.*, **14**, 6805–6847. Available at: http://www.ncbi.nlm.nih.gov/pubmed/23531539 [Accessed May 23, 2018].

Vishwakarma, A., Bashyam, L., Senthilkumaran, B., Scheibe, R. and Padmasree, K. (2014) Physiological role of AOX1a in photosynthesis and maintenance of cellular redox homeostasis under high light in Arabidopsis thaliana. *Plant Physiol. Biochem.*, **81**, 44–53. Available at: https://pubmed.ncbi.nlm.nih.gov/24560882/ [Accessed February 12, 2021].

Wang, Y., Berkowitz, O., Selinski, J., Xu, Y., Hartmann, A. and Whelan, J. (2018) Stress responsive mitochondrial proteins in Arabidopsis thaliana. *Free Radic. Biol. Med.*, **122**, 28–39. Available at: https://pubmed.ncbi.nlm.nih.gov/29555593/ [Accessed March 8, 2021].

Wang, Y., Lyu, W., Berkowitz, O., et al. (2016) Inactivation of Mitochondrial Complex I Induces the Expression of a Twin Cysteine Protein that Targets and Affects Cytosolic, Chloroplastidic and Mitochondrial Function. *Mol. Plant*, **9**, 696–710. Available at: http://linkinghub.elsevier.com/retrieve/pii/S1674205216000113 [Accessed May 23, 2018].

Wang, Y., Selinski, J., Mao, C., Zhu, Y., Berkowitz, O. and Whelan, J. (2020) Linking mitochondrial and chloroplast retrograde signalling in plants. *Philos. Trans. R. Soc. Lond. B. Biol. Sci.*, **375**, 20190410. Available at: http://www.ncbi.nlm.nih.gov/pubmed/32362265 [Accessed March 9, 2021].

Wu, G.-Z. and Bock, R. GUN control in retrograde signaling: How GENOMES

UNCOUPLED proteins adjust nuclear gene expression to plastid biogenesis. Available at: https://academic.oup.com/plcell/pages/General-Instructions [Accessed December 13, 2021].

Tables

Table S1: Microarray-based relative gene expression profiling (total, plastidial mitochondrial and total with p-values<0.05) of rifampicin-treated *versus* untreated etiolated WT seedlings.

Table S2: Primers used in qPCR expression analyses.

Table S3: GC-MS relative metabolomic profiling and amino acid quantification using OPA-HPLC profiling in rifampicin-treated *versus* untreated etiolated WT seedlings.

Figure Legends

Fig. 1 Limitation of PGE interferes with skoto-morphogenesis (A) and photo-morphogenesis (B). A) Top panel: Dissection microscope images of etiolated WT seedlings grown in the presence of DMSO (as a mock control for rifampicin), rifampicin (RIF) 200 µg/ml, spectinomycin (SPEC) 250 µg/ml or 1-aminocyclopropane-carboxylic acid (ACC) 20 µM and mutant *rpoTp* seedlings. Scale bar corresponds to 2 mm. **Middle panel**: Box-plots of median values of apical hook angle measurements. The number of pooled individuals (N, measured in 4 independent analyses) corresponds to 137 seedlings for WT + DMSO and 156 for WT + RIF; N (measured in 4 independent analyses) corresponds to 122 seedlings for WT and 135 for WT + SPEC; N (measured in 7 independent analyses) corresponds to 252 seedlings for WT and 246 for *rpoTp*; N (measured in 3 independent analyses) corresponds to 82 seedlings for WT and 115 for WT + ACC. The differences between treated and untreated seedlings or between *rpoTp* seedlings and WT that are significant by statistical tests are indicated by asterisks (***P<0.001). **Bottom panel**: The apical hook curvature was measured as the angle (blue line) that is formed by the two straight lines (red) passing through the hypocotyl and the cotyledon axes. Any hook angle larger than 180° was considered as twisted. **B) Top panel**: Dissection microscope images of etiolated *cop1-4* seedlings grown in the presence of DMSO (as a mock control for rifampicin), rifampicin (400 µg/ml), spectinomycin (500 µg/ml) and ACC (20 µM). Scale bar corresponds to 0.5 mm. **Middle panel**: Box plots of median values of cotyledon separation angle measurements. The number of pooled individuals (N) that were measured in 2 independent cotyledon angle analyses corresponds to 62 seedlings for *cop1-4*+DMSO, 44 for *cop1-4*+RIF 200 and 67 for *cop1-4*+RIF 400; to 74 for both *cop1-4* and *cop1-4*+ACC; the number of pooled individuals (N) that were measured in 3 independent hook angle analyses corresponds to 61 for *cop1-4* and 51 for *cop1-4*+SPEC (500 µg/ml) seedlings. The differences between treated and untreated seedlings that are significant by statistical tests are indicated by

asterisks (***P<.001). **Bottom panel**: The cotyledon separation angle was measured as the angle (blue line) that is formed by two straight lines (red) passing through the cotyledon axes.

Fig. 2 Relative gene expression and metabolic profiles of rifampicin-treated *versus* control WT etiolated seedlings. **A)** Relative expression values for the 10 most up-regulated genes in rifampicin-treated etiolated WT seedlings are presented as log2-fold changes (FC) together with the corresponding p-values, which are derived from a t-test adjusted for false discovery rate (FDR) after the Benjamini-Hochberg (BH) procedure (BH adj. *p*-value). Gene and protein identities are indicated together with the cellular localization (mitochondrial (mt), plastidial (pt), cytoplasmic (cyt), uncharacterized (un)) and function ("Mt stress" stands for "response to mitochondrial stress"). On the right side, it is indicated when the genes are also found among the most ten up-regulated genes in etiolated mutant *rpoTmp* seedlings (Merendino *et al.*, 2020). **B)** Distribution of relative expression values for mitochondrial, nuclear and plastidial genes in rifampicin-treated etiolated WT seedlings. Given values represent log2FC. The log2FC of mitochondrial transcripts in seedlings treated with RIF were globally higher than nuclear transcripts (Wilcoxon p-value <2e-16). The log2 FC of plastidial transcripts in seedlings treated with RIF were globally lower than nuclear transcripts (Wilcoxon p-value = 4.351e-06). **C**) Log2 FC of expression levels of plastidial, mitochondrial and nuclear genes in RIF-treated WT seedlings *versus* untreated seedlings determined by RT-qPCR. The expression levels were normalized to the mean of *PP2A* (nuclear) expression, used as a reference gene. The mean values of two biological replicates are plotted. Error bars correspond to standard errors. T-test was performed to determine the statistical significance of the data (T-test, *= p-value 0.05; **=0.01). **D**) Metabolic Heat Map of control (DMSO) and rifampicin-treated seedlings (RIF) by MEV software. In total, the levels of 49 metabolites were significantly affected by RIF treatment (T-test, p-value 0.05); the amounts of 47 metabolites were increased while two metabolites decreased. Metabolomic profiling of five repetitions (R1-5) was performed using Gas Chromatography-Mass Spectrometry (GC-MS). The intensity of the red-green color indicates the metabolite abundance levels compared to the median value: the green color represents the trend of decrease; the red corresponds to the increase. The clustering allows to group metabolites with similar variations towards median. The top to the bottom clustering of metabolites is based on pair-wise similarity.

Fig. 3 The impact of PGE limitation on hook bending is independent of the ANAC017- and GUN1-dependent organelle retrograde pathways and of the EIN2-dependent

signalling pathway. A) Log2 FC induction of expression levels of mitochondrial stress marker genes in RIF-treated WT and mutant *anac017* seedlings *versus* corresponding untreated seedlings determined by RT-qPCR. The expression levels were normalized to the mean of *PP2A* expression, used as a reference gene. The mean values of two biological replicates are plotted. Error bars correspond to standard errors. **B) Top panel:** Dissection microscope images of etiolated *anac017* seedlings grown in the presence of DMSO as a mock control for rifampicin and rifampicin (RIF) 200 µg/ml. **Bottom panel:** Box plots of median values of apical hook angle measurements. The number of pooled individuals (N) that were measured in 2 independent hook angle analyses corresponds to 40 seedlings for WT+DMSO and 44 for WT+RIF; to 46 for *anac017*+DMSO and 54 for *anac017*+RIF. The differences between treated and untreated seedlings that are significant by statistical tests are indicated by asterisks (***P<.001) **C) Top panel**: Dissection microscope images of etiolated *gun1-201* seedlings grown in the presence of DMSO or rifampicin (RIF) 200 µg/ml. **Bottom panel**: Box plots of median values of apical hook angle measurements. The number of pooled individuals (N) measured in 2 independent hook angle analyses corresponds to 40 seedlings for WT+DMSO and 41 for WT+RIF; to 54 for *gun1-201*+DMSO and 46 for *gun1-201*+RIF. The differences between treated and untreated seedlings that are significant by statistical tests are indicated by asterisks (***P<.001) **D) Top panel**: Dissection microscope images of etiolated *ein2-1* seedlings grown in the presence of DMSO, rifampicin (RIF) 200 µg/ml or ACC 20 µM. **Bottom panel**: Box plots of median values of apical hook angle measurements. The number of pooled individuals (N) that were measured in 2 independent hook angle analyses corresponds to 36 seedlings for WT + DMSO and 37 for WT + RIF (100 µg/ml); to 43 for *ein2-1* + DMSO and 29 for *ein2-1* + RIF (100 µg/ml); N (measured in 2 independent analyses) corresponds to 30 seedlings for WT + DMSO and 42 for WT + RIF (200 µg/ml); to 50 for *ein2-1* + DMSO and 62 for *ein2-1* + RIF (200 µg/ml). N (measured in 2 independent analyses) corresponds to 73 seedlings for WT and 79 for WT + ACC; to 33 for *ein2-1* and 36 for *ein2-1* + ACC. The differences between treated and untreated seedlings that are significant by statistical tests are indicated by asterisks (***P<.001).

Fig.4 Impact of AOX1A genetic abolishment on the apical hook bending under plastid gene-expression inhibitory conditions. A) Analysis of AOX1A protein content used as a marker for mitochondrial stress. Protein extracts (20µg) from etiolated WT seedlings grown in the presence of DMSO or rifampicin (RIF) 200 µg/ml were separated by SDS-PAGE and immunoblotted with specific antisera against mitochondrial AOX protein (nuclear-encoded)

and the vacuolar protein ATPase (nuclear-encoded) as a loading control. **B)** Capacity of the AOX-dependent pathway in etiolated WT seedlings grown in the absence or presence of rifampicin (RIF) 200 µg/ml. AOX capacity was calculated upon addition of 1 mM (final concentration) KCN to the measurement cell and shown as the % ratio of KCN-insensitive O_2 consumption rate to total O_2 consumption rate. Median values (thick horizontal lines) of N independent measurements (full circles) were scatter-plotted for WT (N=7) and WT+RIF (N=9). **C)** Phenotypic analysis of RIF-treated *aox1a* mutant seedlings. **Left panel**: Zoomed dissection microscope images of RIF (200 µg/ml)-treated *aox1a-1* seedlings showing twist and untwist phenotypes. The untwisted class comprises seedlings with hooks that are either sharp (hooked) or round (comma). **Right panel:** Percentage of the WT, *aox1a-1* and *aox1a-2* seedlings grown on rifampicin (200 and 400 µg/ml) and showing either twist or untwisted phenotype. The number of pooled individuals (N) measured in 2 independent hook angle analyses corresponds to 83 for WT+RIF200, 132 for WT+RIF400, 69 for *aox1a-1*+RIF200, 160 for *aox1a-1*+RIF400, 120 for *aox1a-2*+RIF200 and 164 for *aox1a-2*+RIF400 seedlings. **D)** Microscope images of NBT-stained WT, *aox1a*-1 and *aox1a-2* seedlings, that were grown in control conditions or in presence of RIF 400.

Fig. 5 Scheme of the proposed functional link between PGE limitation and skoto-morphogenic reprogramming. In etiolated rifampicin- or spectinomycin-treated WT seedlings, transcription of the PEP-dependent plastid genome or translation of plastid transcripts is limited, respectively. As consequence, ROS are accumulated in the cell, either in etioplasts and/or mitochondria, nucleus cytoplasm, leading to (red discontinuous arrows) transcriptional induction of nuclear genes that are considered as markers for mitochondrial stress (thick black arrow, *AOX1A*, *AT12CYS*, *NDB4* and *UPOX*). If nuclear gene-expression is directly regulated by plastid dysfunction or *via* mitochondrial stress is still unknown (red arrows). The activation of nuclear gene expression is independent of both the GUN1-plastidial and the ANAC017-mitochondrial retrograde pathways and might be supported by yet unknown factors. Expression of AOX is increased also at the protein level (thick discontinuous black arrow) and consequently, the capacity of the AOX-dependent chain is augmented and more electrons can be diverted by this pathway. Role of AOX consists in detoxifying the cell from ROS. As an ultimate effect, a developmental response (twisting phenotype) is induced. If and how the developmental response is triggered directly by plastid signals or *via* mitochondria by AOX-generated signals is still unknown (thin discontinuous black arrows, online version in color).

Figure S1: The effect of PGE limitation is restricted to skoto-morphogenesis *in sensu stricto.* A) Etiolated WT seedlings were grown on nitrocellulose membrane filters either on MS agar plates in the absence of rifampicin (A) or on rifampicin-containing MS agar plates since the beginning of stratification (B) or on MS agar plates and then transferred (on the filter) to rifampicin-containing MS agar plates before light exposure (C) or at the beginning of dark-growth (D). The continuous black line indicates the length of the RIF treatment during the growth protocol. **B)** The percentage of seedlings exhibiting hook bending higher than 180° (twist) in a single experiment is reported.

Figure S2: Gene expression analysis by RTqPCR and microarray techniques. A) Gene ontology sub-grouping of deregulated genes (DEG) in rifampicin-treated *versus* untreated dark-grown WT seedlings, with relative expression values (log2 fold change) >0 (UP, left panel) or <0 (DOWN, right panel) and p-values<0.05 (Table S1). Significantly enriched biological processes following analysis of the gene array data are clustered together using ShinyGO. FDR is adjusted from the hypergeometric test. Fold Enrichment is defined as the percentage of UP or DOWN DEGs belonging to a specific pathway, divided by the corresponding percentage in the background. FDR tells how likely the enrichment is by chance; Fold Enrichment indicates how drastically genes of a certain pathway is overrepresented. **B)** The expression of a selected group of genes was analyzed by both microarray (Table S1) and RT-qPCR (Fig 2C). The log2FC ratios of these transcripts are given for the two techniques.

Figure S3: Analysis of plastid specificity for the spectinomycin antibiotic. Analysis of S7 and NAD9 protein contents used as plastidial and mitochondrial markers, respectively. Protein extracts (100µg) from etiolated WT seedlings grown in absence or in presence of spectinomycin (Spec) 250 and 500 µg/ml were separated by SDS-PAGE and immunoblotted with specific antisera against plastidial-encoded S7 and mitochondrial-encoded NAD9 proteins and the vacuolar protein ATPase (nuclear-encoded) as a loading control. Quantification of the S7 and NAD9 signals was performed by the ImageLab software using ATPase for normalization and values were reported in the bottom panel (ND: not detected).

Figure S4: Schematic representation of metabolite ratio by GC-MS and amino acid quantification by OPA-HPLC in untreated and RIF-treated WT seedlings. A) In case of metabolite ratios, units are arbitrary, while for amino acids levels the units are pmol/mg FW.

Statistical significance of differences in metabolite abundance between control and RIF-treated seedlings was verified using the Student's T-test and a significance value of $P \leq 0.05$. Asterisks stand for $P<0.05$(*), $P<0.01$(**), $P<0.001$(***). **B)** Total amino acid levels are represented for control and RIF-treated seedlings.

Figure S5: Relative expression values for A) PhANGs and B) genes involved in ethylene biosynthesis and signalling pathways in rifampicin-treated *versus* untreated etiolated WT seedlings. Values are given as log2FC together with the corresponding p-values, which are derived from a t-test adjusted for false discovery rate (FDR) after the Benjamini-Hochberg (BH) procedure (BH adj p-value). Gene and protein identities and function (synthesis or signaling) are also indicated. SAM: S-adenosyl methionine synthase; ACS: ACC synthase; ACO: ACC oxidase. **C)** Ethylene emission levels from 500 mg (fresh weight) of WT etiolated seedlings grown either in the presence of DMSO as a mock control for rifampicin or with rifampicin (RIF) 200 µg/ml. The plot shows the measured ethylene levels in ppbv (parts per billion) during a relative time since the start of the experiment.

Figure S6: Total O_2 consumption rate in etiolated WT plants grown in the presence or absence of rifampicin. Median values (thick horizontal lines) of N independent measurements (full circles) were scatter-plotted for mock (N=7) and rifampicin (200 µg/ml)-treated (N=9) WT seedlings.

Figure S7: Dissection microscope images of etiolated *aox1a-1* and *aox1a-2* seedlings. A) Allelic mutant seedlings, *aox1a-1* and *aox1a-2*, were grown either in absence or in the presence of DMSO as a mock control for rifampicin, with rifampicin (RIF) 200 µg/ml or spectinomycin (SPEC) 500 µg/ml. RIF- and SPEC-treated *aox1a* mutant seedlings show twist, hook or comma phenotypes (Fig. 4C). **B)** Dissection microscope images of *aox1a-2* mutant seedlings that were grown on RIF400 for 4 days in the dark or **C)** for 10 days in the dark and then transferred 8 days in the light. Seedlings in B) present comma (1, 2) and twist (3) phenotypes.

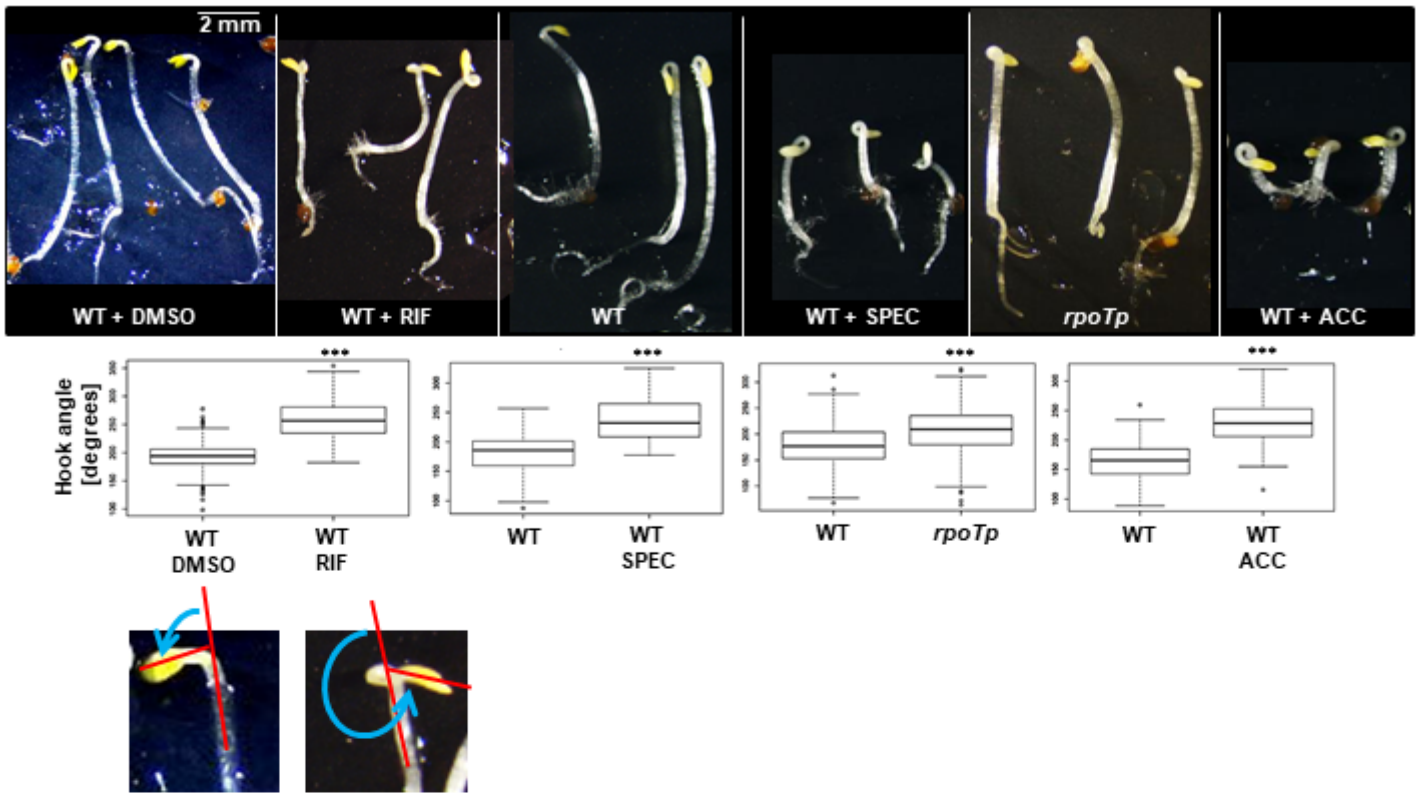

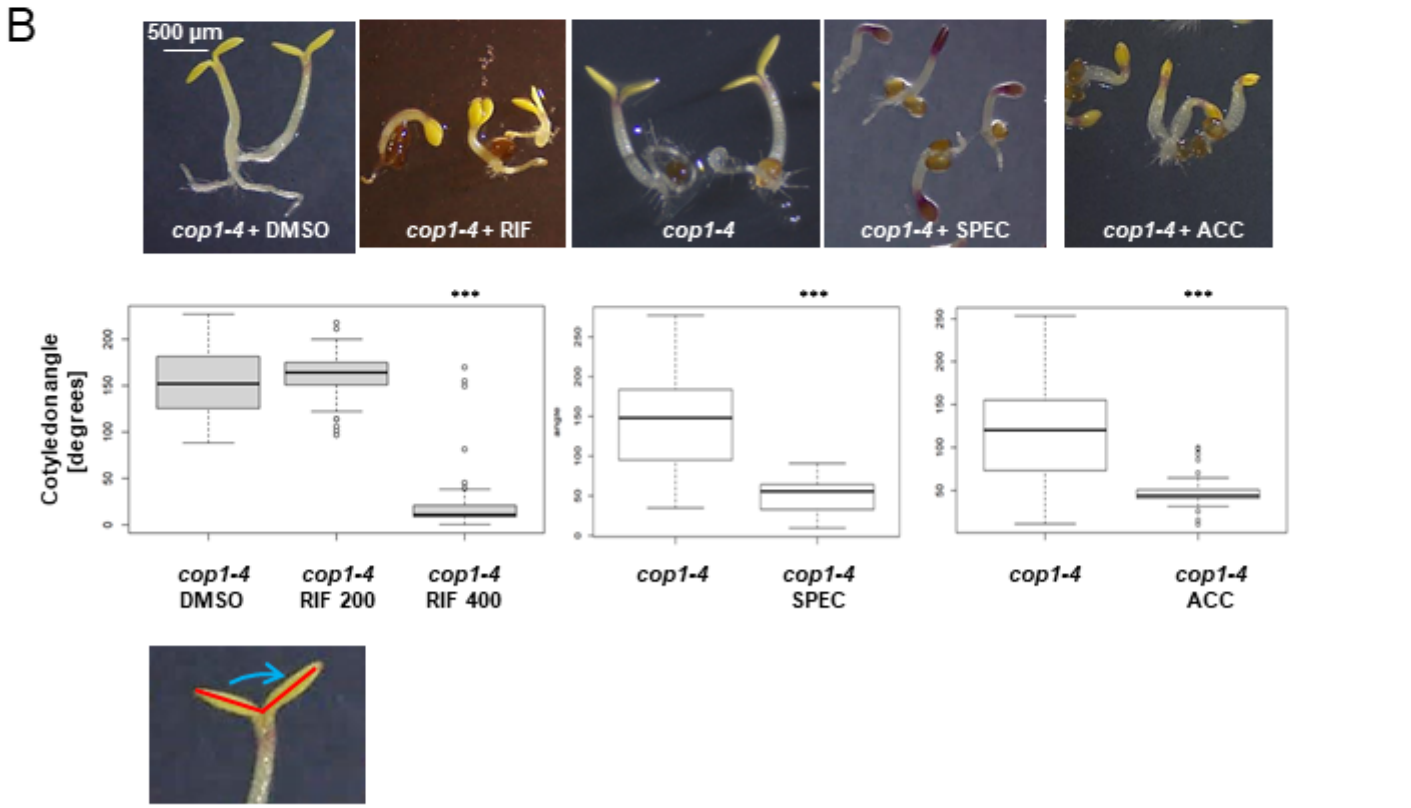

Fig. 1

A

	gene	WT+Rif/WT log_2FC	BH adj. *p*-value	protein	localization	function	*rpoTmp*/WT (top10)
1	at5g09570	4,5	6,52E-05	AT12CYS-2, Twin Cysteine Protein	mt/pt	**Mt stress**	X
2	at5g54100	3,1	6,52E-05	SLP2, protein phosphatase	mt	**Mt stress**	X
3	at5g54560	3,0	3,01E-03	ATDOB13 (DUF 295)	mt	**Mt stress**	X
4	at2g20800	2,9	1,17E-03	NDB4, external alternative NAD(P)H dehydrogenase	mt	**Mt stress**	X
5	at5g54450	2,9	9,14E-04	ATDOB11 (DUF 295)	mt	**Mt stress**	
6	at5g52940	2,8	7,63E-04	ATDOB5 (DUF 295)	mt	**Mt stress**	X
7	at5g09520	2,8	5,15E-03	hydroxyproline-rich glycoprotein family protein	cyt	**Gly-Pro rich**	X
8	at1g74110	2,8	1,42E-03	CYP78A10, cytochorme P450, oxidation reduction	pt	**Oxido-reduction**	
9	at1g55990	2,6	1,93E-02	glycine-rich protein	un	**Gly-Pro rich**	X
10	at1g64220	2,6	4,11E-03	TOM7-2, translocase of outer membrane 7 kda subunit 2	mt	**Mt functions**	X

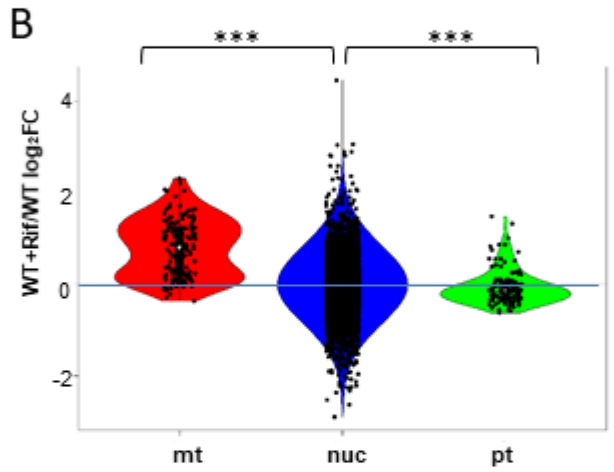

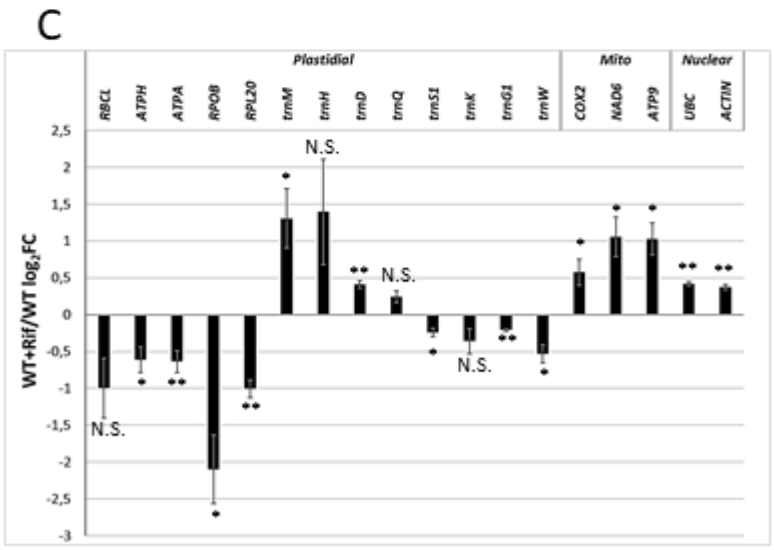

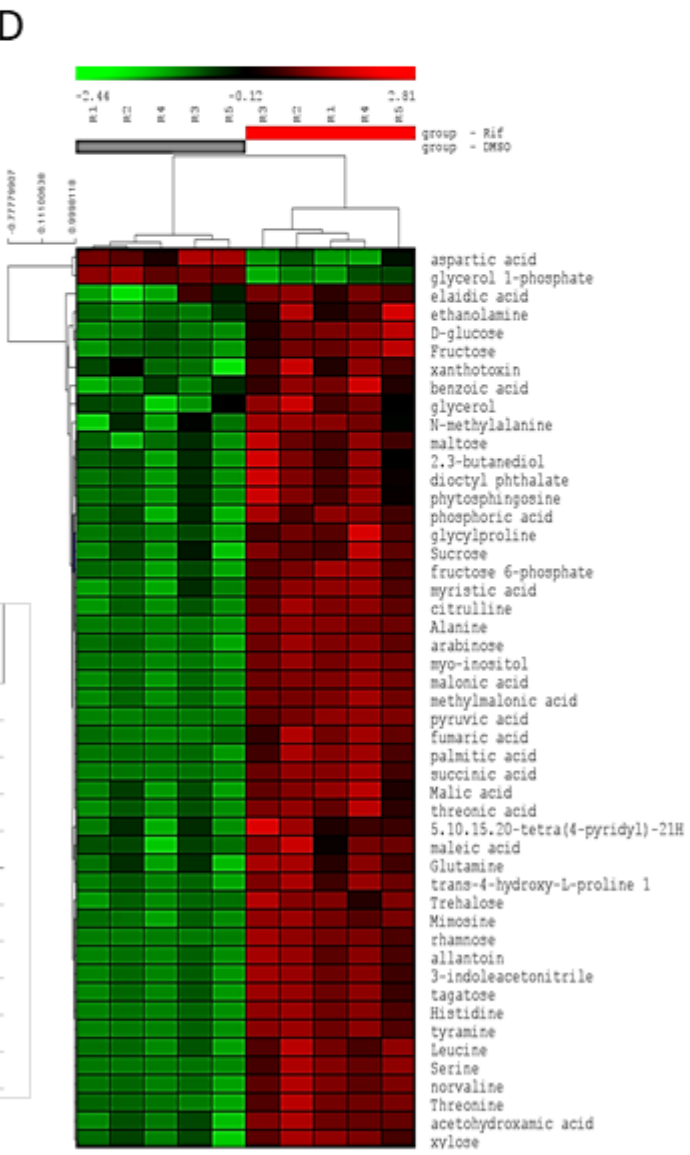

Fig. 2

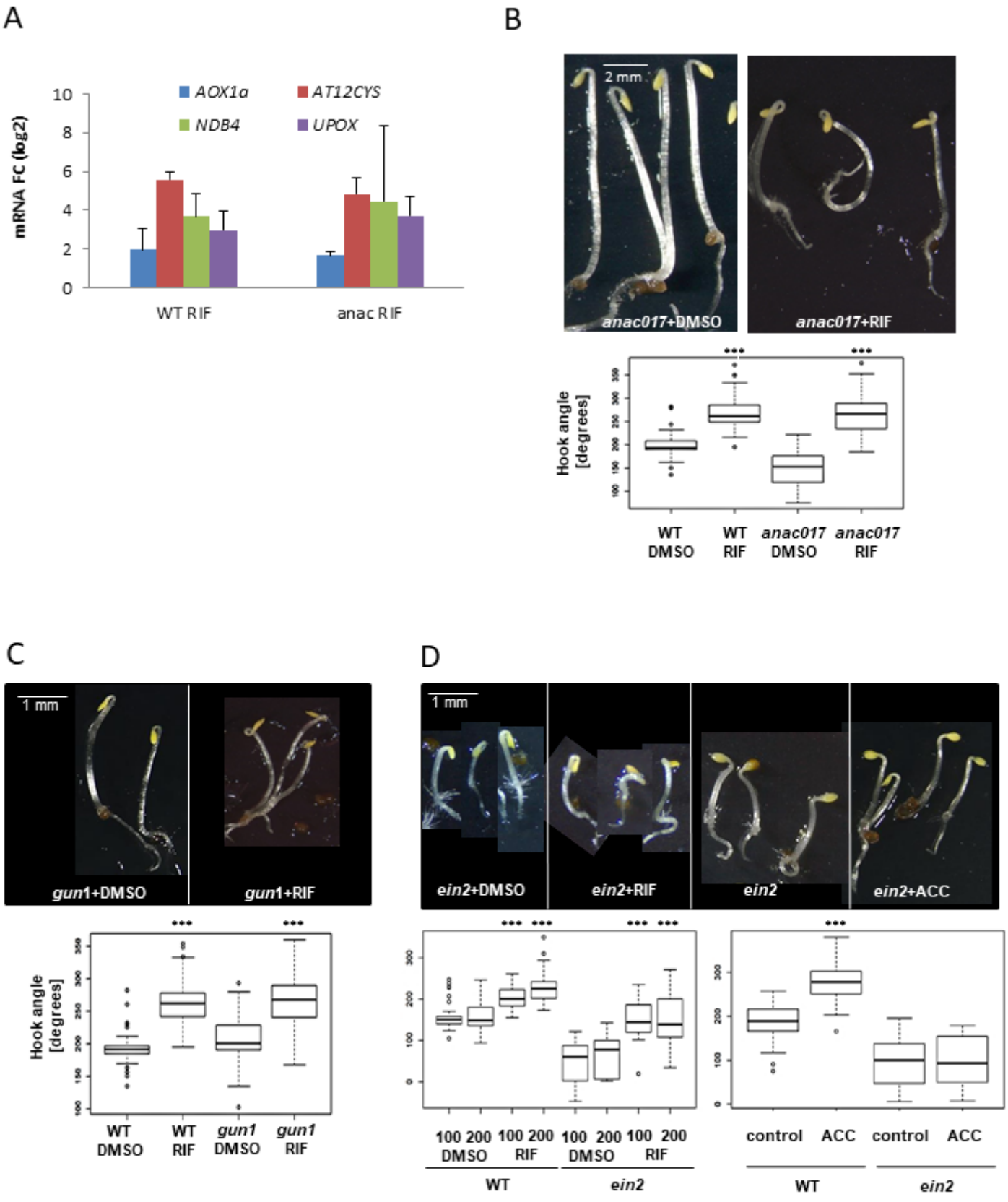

Fig. 3

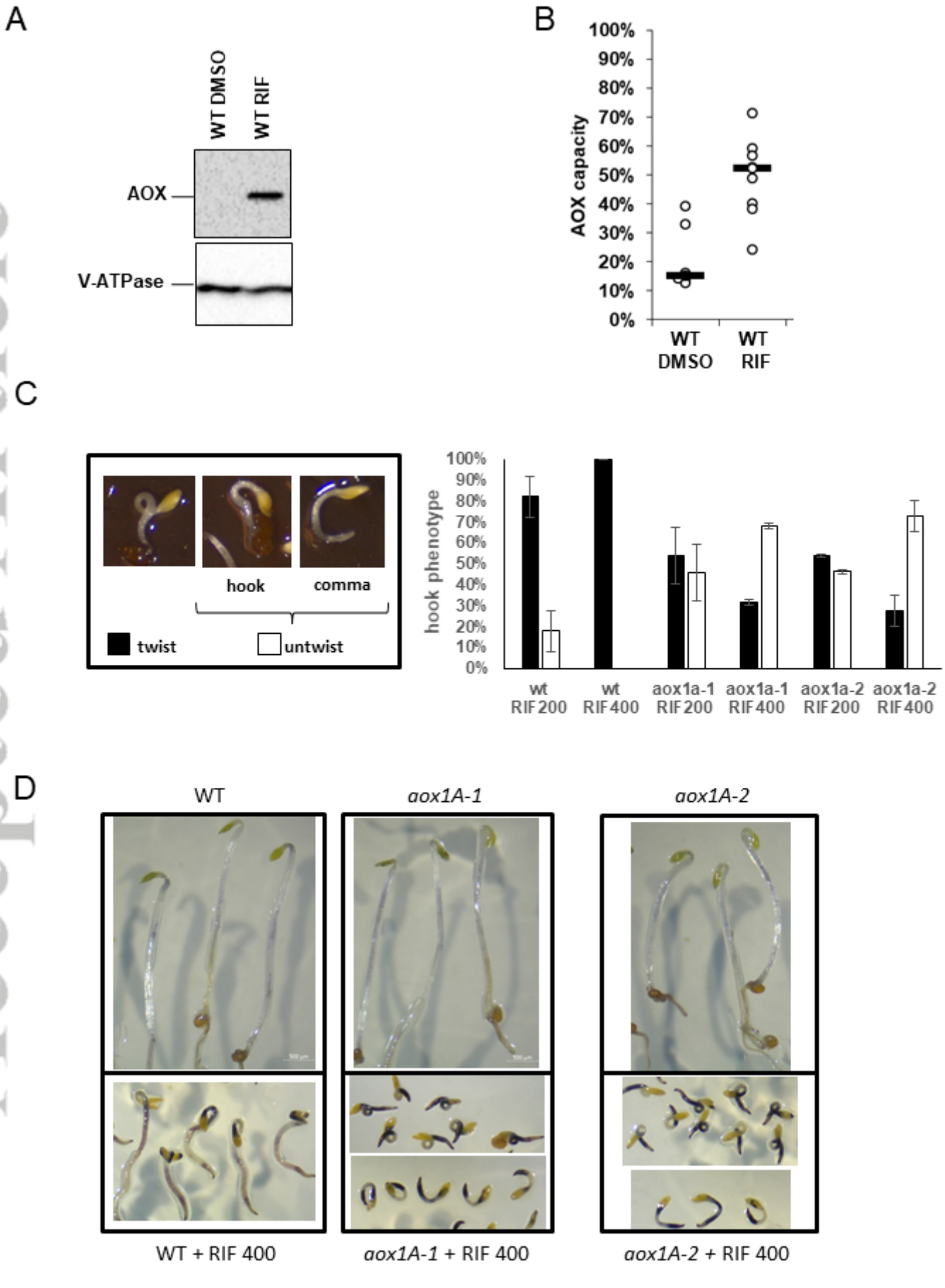

Fig. 4

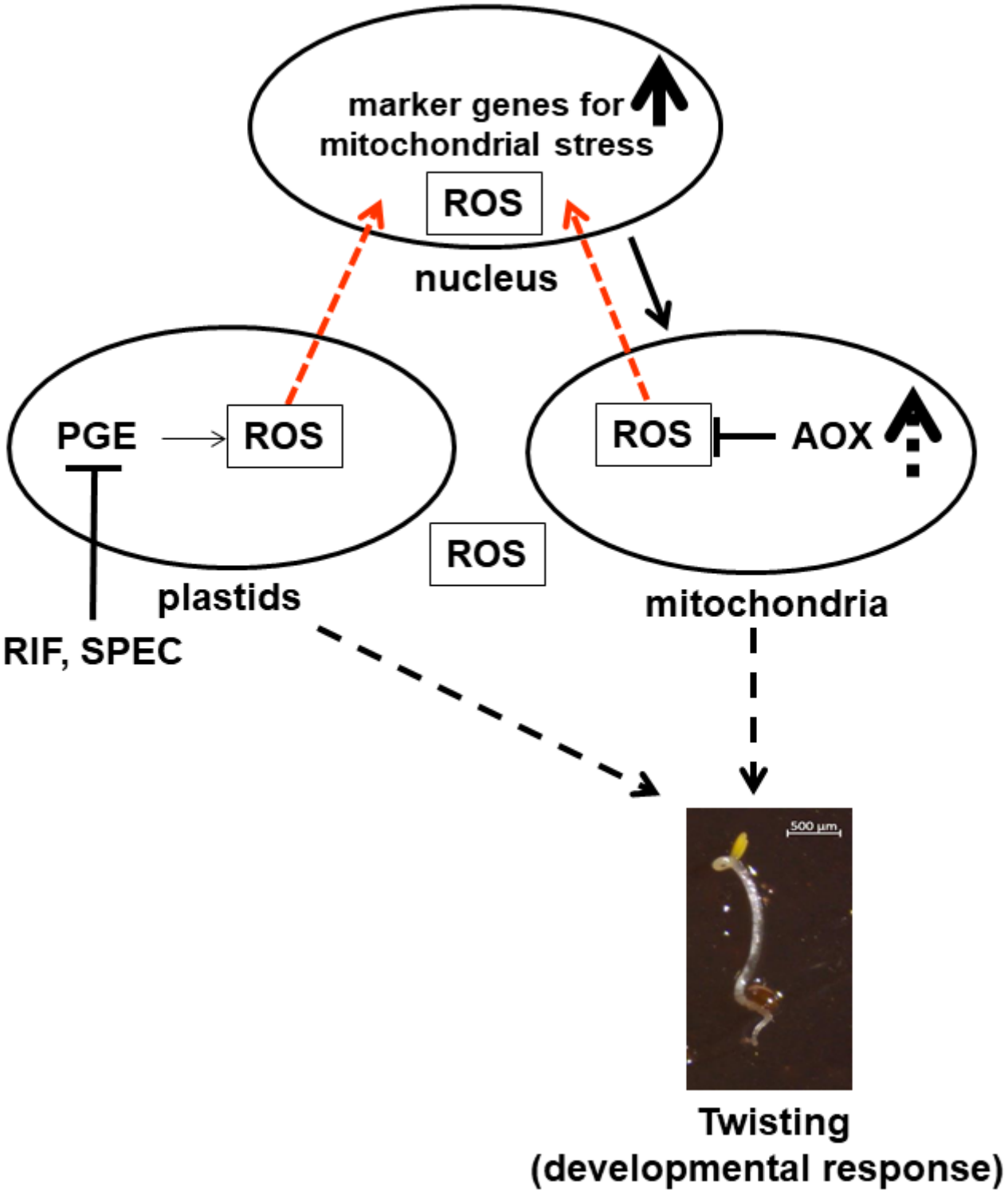

Fig. 5